CHARGE TRANSPORT IN ORGANIC ELECTRONIC DEVICES

A Thesis

Presented to the Faculty of the Graduate School

of Cornell University

in Partial Fulfillment of the Requirements for the Degree of

Master of Science

by

Michelle Kim-Mai Giron

February 2010

ABSTRACT

Organic materials are currently being examined for their potential use as active conducting media in electronic devices. Computational methods were used to study the transport characteristics across single organic molecules and through organic molecular crystals as well as the possibility of chemical impurities in crystals. In particular, the dependence of conductance on the central dihedral angle of single molecule junctions containing 4,4'-diaminobipenyl derivatives was probed by combining electronic structure calculations with a tunneling model and comparing to experimental results from literature. The calculations and model were adequate in reproducing the trend observed in experiment, implying that the differences in conductance across this class of molecules can be attributed mainly to the central dihedral angle. A method for calculating hole mobilities in organic molecular crystals at room temperature was considered for crystals of pentacene, tetracene, and anthracene. Computed mobilities were found to have a sensitive dependence on the calculated parameters and to insufficiently predict mobility trends across the materials. Impurities of water molecules in surface vacancy defects of pentacene crystals were studied through the use of molecular dynamics. Water molecules were found to bind to these defects, which has implications for charge transport through pentacene crystals.

BIOGRAPHICAL SKETCH

Michelle Kim-Mai Giron was raised in Los Angeles, California in a family of four gregarious children. She attended Catholic primary and secondary schools before entering her undergraduate studies at the California Institute of Technology, where she earned a degree in chemical engineering. Graduate studies brought her to Cornell University, where she continued academic work in the field of chemical engineering. She presently resides and works in Orange County, California.

To my good friend Kamalah.

ACKNOWLEDGEMENTS

There are several individuals to whom I owe my gratitude for making this work possible. I wish to thank my advisor, Professor Paulette Clancy, for providing guidance and support throughout my graduate studies and for allowing me to undertake challenging research. I thank my minor advisor, Professor John Marohn, for many thoughtful conversations and the experimental perspective of my computational work. I am grateful to my group members, especially Dr. Mohit Haran, Joseph Goose, and James Catherwood, for lending their expertise during the course of my research. I also thank Professor Garnet Chan, Professor Richard Hennig, and my friend Dr. Sina Yeganeh for sharing their knowledge and providing additional assistance in my efforts. I offer appreciation to my siblings Marie, Angela, and Philip for their continued encouragement. Lastly, I acknowledge my mother and father for the importance they placed on my education and for the many ways in which they have taught me.

TABLE OF CONTENTS

LIST OF TABLES

LIST OF FIGURES

CHAPTER 1

INTRODUCTION

Over the past two decades, there has been an interest in incorporating organic materials into the active components of electronic devices, through which the movement of charge occurs. Though many examples of charge transport through organic molecules exist in the biological systems seen in nature, organic materials used in fabricated devices have mainly been limited to supportive capacities, such as photoreceptors for photocopying [1], photoresists for lithography, packing materials for chips, and device insulators. Aviram and Ratner's theoretical proposal of a molecular rectifier sparked interest in the possibility of single-molecule devices [2], but it was Koezuka *et al.*'s report of an electronic device based on polythiophene that demonstrated organic materials' potential in devices similar to the common field effect transistor [3]. Bulk organic materials had long been studied for their potential use as active conducting media [4] (and field effect). After decades of speculation and development, functioning organic devices have been fabricated and are now available commercially in products such as watches, cell phones, and displays, and active research areas include passivation of wires by organic monolayers, semiconducting polymers, molecular wires and switches, conducting organic thin films, organic light-emitting diodes, and organic solar cells.

Organics are being exploited for a variety of reasons: with the extensive knowledge of organic chemistry and synthesis currently available, there are myriad possibilities for compounds that can be chosen and chemically tuned for specific purposes in a device. For example, organic compounds with deliberate sizes have already been used in cross-wire contacts [5], and they have

been the key components of chemical sensors based on field effect transistors [6]. Organic materials are also attractive for their relative low cost, both in raw materials and processing. Fabrication steps involving organic materials can be accomplished at lower energy input than those of inorganic materials. In addition, their mechanical properties make organics suitable for novel device features such as flexibility.

For all their potential, organic materials pose many challenges in research and device use. Theories of carrier transport are not well-developed, and charge separation in bulk organic materials is not well-understood. The combination of theory and computation has so far proven weak in predicting the experimentally observed differentials in conduction among materials. Coupled with difficulties in manufacturing control, irreproducibility of characterization experiments, and device degradation, practical utilization becomes fraught with even more obstacles. A pointed effort to fully realize the possibilities of organic devices will involve making quantitative connections between a material's structure and its experimentally observed function in a bottom-up manner. This ideally entails prediction of the material structure and the electronic properties prior to experiment, but both remain challenging problems to address.

The field of organic electronics is broad, encompassing many different material choices (polymers and small molecules) and devices (i.e. organic LED's, single molecule wires, and transistors). This thesis primarily focuses on computational study of electronic properties in the following organic mediums: molecular wires and molecular crystals composed of small molecules. In addition, structural studies of defects in organic molecular crystals are presented. The next chapter deals with molecular wires, the most basic system in organic

electronics, and treats the interesting case of 4,4'-diaminobiphenyl and related derivatives. Here, an explanation of the connection between molecular structure and conductance is attempted. The subsequent chapters cover charge transport in crystals of pentacene and smaller acenes, which have been used as standards in organic electronic devices, and seek to uncover the mechanisms of charge transport within bulk materials. Computation provides a link between theoretical models and experiment, and its appropriateness for these systems will be considered.

CHAPTER 2

CHARGE TRANSPORT THROUGH MOLECULAR WIRES: 4,4'-DIAMINOBIPHENYL

At its most basic level, molecular electronics involves the passage of charge through a single molecule between two electrodes. How a molecule's geometry and its interface with the electrodes affect charge transport is the fundamental question, as it is necessary to demonstrate the molecule's specific contribution to the device's resistance and to form guidelines for choosing molecules for specific applications. Rationalizing the role of the molecular structure in the functioning of the wire remains challenging because the system is necessarily out of equilibrium during transfer events. In conventional inorganic wires, conduction occurs at steady-state through a bulk material, and minor lattice defects negligibly impact average transport characteristics. In contrast, conduction through molecular wires is the sum of individual charge transfer events across the electrodes: rates of transfer are sensitive to contact geometry along with molecular geometry, both of which may shift during the charge transfer – the transition state. Determining experimentally or theoretically these out-of-equilibrium geometries is not possible, given available computing resources. Moreover, since these systems obviously require quantum mechanical considerations at the single-molecule level, theoretical treatments are complicated by many factors. Nevertheless, even the most basic models can shed light on the differences in conductance for related molecules.

This chapter focuses on structure and function relationships for a set of molecular wires based on biphenyl derivatives. In particular, the role of the π-system orbitals in determining transport properties across the set is probed.

Studying particular geometrical features and functional groups allows for possible application to more complex molecules that incorporate several chemical groups. A simple model of charge tunneling across wires is considered using density functional theory and semiempirical calculations. The motivation for this research is recent experimental work [7] indicating that the the extent of π-conjugation across the two phenyl rings in the molecules, described by their central dihedral angle, is the primary modulator of conduction through the molecular wire. The computation presented here gives insight that experiments alone cannot offer. There are two major questions this research seeks to answer: what is the configuration of the molecules during conductance measurements, and how does the conductance depend on the twist angle of the diaminobiphenyl backbone?

2.1 Tunneling in 4,4'-Diaminobiphenyl Derivatives

Transport characteristics of molecular wires are affected by several factors, including molecular length and configuration, bonding interactions between molecule and electrode, Coulomb repulsion, and thermal energy [8]. The variability of processing conditions leads often to irreproducible results, and regardless, rationalizing bonding and geometry at molecule-electrode interfaces remains a challenge. Current-voltage curves can show how the electronic states of the electrodes couple with both the electronic and vibrational states of the bridging molecule [8], and spectroscopic methods such as inelastic electron tunneling spectroscopy can reveal the signatures unique to a particular ligand [9]. In this particular case study, gold break junctions bridged by 4,4'-diaminobiphenyl derivatives were used to determine the chemical "signature" of a particular

molecule as related to its twist angle. In contrast to spectroscopic methods that scan across a range of frequencies or voltages, here the applied voltage was fixed to probe the influence of molecular geometry on conductance.

Venkataraman and co-workers [7] chose to study molecular wires based on the biphenyl molecule (see Figure 2.1(a)) because these wires are a basic system for measuring structure-function relationships of π-conjugated systems. When a weak voltage is applied across the length of a biphenyl molecule between electrodes, conduction is mediated mostly by the molecule's frontier orbitals, which lie in the phenyl groups' conjugated π-system, because these orbitals have energies closest to the work function of the metallic electrodes. The dihedral angle describing the angle between the planes of the two phenyl rings is a measure of the extent of π-conjugation in the molecule: a molecule with two coplanar phenyl rings has the highest measure of π-conjugation and that with perpendicular phenyl planes has essentially negligible π-conjugation.

Substituted 4,4'-diaminobiphenyls (see Figure 2.1(b)) were chosen in particular because their break-junction signals had little noise and were within a narrower range as compared to molecules with other terminus groups (i.e. thiol and nitrile groups). Venkataraman *et al.* propose that the superiority of the amine group in break-junction experiments is due to the specificity with which terminus amines bond to under-coordinated Au atoms on the tip surface and substrate [10]. A thiol group, in contrast, can have a variety of strong bonding configurations with a gold surface, leading to a broad range of comparably noisier conductance traces.

The set of diaminobiphenyl derivatives incorporated side groups into the *meta* and *ortho* positions of the phenyl groups so that the average twist angles

for each molecule were held on average at various and unique values from 0° to 180°. Conductances through this set of molecules in solution were shown to clearly depend on the twist angle: the authors reported that at an applied voltage of 0.025 V (across a single molecule of length ≈ 10Å), conductance decreased as the twist angle increased from coplanar phenyls to out-of-plane phenyls, evidence for transport mediation through the π-system of the molecules. A schematic of their experiment is shown in Figure 2.2.

The low voltage used in the break junction experiment was not high enough to significantly affect the energy levels within the molecule at the junction, and consequently, the molecule can be seen to be a tunneling barrier for the conducting charge [8]. Assuming weak electronic coupling between the bridging ligand and the metal contacts, the conductance across a molecular wire is given by [11][12]:

$$g \approx \frac{8e^2}{\pi \Gamma_D \Gamma_A F} k_{D\to A} \tag{2.1}$$

where Γ_D and Γ_A are the inverse lifetimes of an electron residing on the donor and acceptor electrodes, respectively; F is the thermally averaged, Franck-Condon weighted density of nuclear states; and $k_{D\to A}$ is the classical Marcus rate equation for an electron transfer event, given by [13][14][15]:

$$k_{D\to A} = \frac{2\pi}{\hbar} \left|\left\langle \psi_f \left| H \right| \psi_i \right\rangle\right|^2 \left(\frac{1}{4\pi\lambda k_B T}\right)^{\frac{1}{2}} \exp\left[\frac{-(\Delta G^\circ + \lambda)^2}{4\lambda k_B T}\right] \tag{2.2}$$

where $\left|\left\langle \psi_f \left| H \right| \psi_i \right\rangle\right|$ is the coupling between the final and initial electronic wavefunctions of the transfer event; T is the temperature; ΔG° is the free energy change of the transfer; and λ is a measure of the nuclear reorganization that occurs in order for a transfer event to occur. The Franck-Condon factor in the rate equation, $(1/4\pi\lambda k_B T)^{1/2} \exp\left[-(\Delta G^\circ + \lambda)^2 / 4\lambda k_B T\right]$, and that of the conductance relationship, F, cancel to reduce the conductance to a relationship that varies with

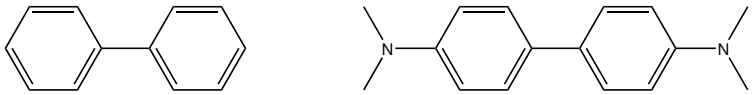

(a) biphenyl (b) 4,4′-diaminobiphenyl

Figure 2.1: Molecules used in molecular wire study

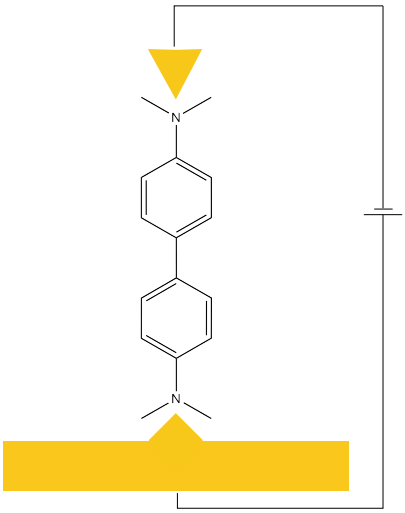

Figure 2.2: Venkataraman *et al.*'s break junction experiment: Au electrode tip makes contact with Au substrate, across which a voltage is applied. When the tip is released from the substrate, a molecule from solution (4,4′-diaminobiphenyl shown here) sometimes bridges the gap between the electrode and substrate, allowing for a conductance measurement. Thousands of conductance traces were measured to determine an average conductance for each of the molecules studied. (Figure adapted from Reference [7].)

the square of the electronic coupling and the reciprocal of the product of inverse lifetimes ($\Gamma_D\Gamma_A$).

Venkataraman *et al.* focus on the electronic coupling, $\langle\psi_f|H|\psi_i\rangle$, and assume that the relative conductances vary with the square of the tunnel coupling between the donor electrode and the bridge molecule. They neglect an analysis of the inverse lifetimes, Γ_D and Γ_A. The tunnel coupling was taken to go as $\cos\theta$, where θ is the twist angle, in reference to the dominant π-π interaction between two $Ru(NH_3)_5$ complexes joined by 4,4'-bipyridine [16]. The researchers found good agreement with the dependence of conductance on $\cos^2\theta$. When the twist angle was 90° (corresponding to $\cos^2\theta = 0$), the conductance nearly vanished.

The exact configuration of the bridge molecules during a conduction event could not be determined experimentally, and it remains a challenging question. Additionally, the linkage between the electrodes and the molecule as well as any stresses on the molecule that occur during the conduction event are difficult to describe. Conduction events are akin to the transition state of a chemical reaction. Since no chemical bonds are made or broken during the transfer, the combination of geometrical optimization and vibrational analysis using computation that could propose a transition state geometry is nearly impossible and would most likely be misleading. Another complication is a molecule's energy surface as a function of twist angle: at room temperature, each molecule has a range of accessible twist angle values.

Thus, the most basic approximation is to take the transition geometries as the ground state configurations of the particular bridge molecule in isolation. Venkataraman *et al.* used such an approximation in their analysis, and their results fit their initial model and implied a dominance of the π-conjugation in

the tunneling events. Here, computational methods similar to that of the experimenters have been used to rationalize this assumption, to shed light on the structure of the molecules in the apparatus. Beyond the previous work, relative rates of electron tunneling across the electrodes with respect to the bridge molecule's twist angle were estimated by using classical electron transfer theory to explain the experimental results.

2.2 Method and Computation

Energy surfaces with respect to the twist angles of 4,4'-diaminobiphenyl and biphenyl, as a comparison, were calculated using density functional theory (DFT), as implemented in Gaussian03[1] [17]. Structures were fully relaxed at the B3LYP/6-31G(d) theory level and basis set while holding the twist angle constant. To simulate electrodes, two gold atoms were placed at both ends of a 4,4'-diaminobiphenyl molecule, and a relaxed scan of the twist angle was again carried out. The LANL2DZ pseudopotential and basis set were used for the Au atoms. An additional *ab initio* scan at MP2/6-31G(d)//B3LYP/6-31G(d) was calculated for biphenyl.[2] All calculations were performed on isolated molecules in vacuum.

Using the resultant energy curve for 4,4'-diaminobiphenyl, a thermal average of the tunneling probability (assumed to be directly proportional to $\cos^2\theta$) was taken at room temperature (300 K) to find the most probable twist angle at which tunneling occurs in the experimental conditions. The energy surface was

[1]Unless otherwise noted, Gaussian03 has been utilized for all density functional theory, *ab initio*, and semiempirical calculations mentioned throughout the text.

[2]The convention used here is [energy calculation method]//[geometry optimization method] and (computational method)/(basis set) within each bracketed set.

first fitted to a 5th order polynomial curve. Boltzmann statistics were then used to obtain thermal averages of the twist angle and tunneling probability.

It follows from the discussion of the conductance relationship that the electronic coupling is the main determinant of the charge transfer rate among the twist angles. To obtain more representative tunneling probabilities, the method outlined by Woitellier, Launay, and Joachim [16] was used to calculate a so-called "effective coupling parameter" (ECP), equivalent to $\langle \psi_f | H | \psi_i \rangle$, as a function of twist angle. The total molecular orbital of the organic ligand and two Au atoms can be described by the form:

$$\psi_n = c_{n1}\phi_1 + c_{n2}\phi_2 + \sum_{\alpha} c_{n\alpha}\phi_\alpha \tag{2.3}$$

where n is the index for the particular system orbital; ϕ_1 and ϕ_2 are basis orbitals of the respective Au atoms; and ϕ_α is an atomic orbital of the ligand. Charge transfer can occur through different channels, which here refer to different pairs of molecular orbitals, ψ_m and ψ_n, representing the initial and final electronic states of the transfer. The rate of transfer between the electrodes represented by single Au atoms is desired, so the ECP is calculated by using total system initial and final molecular orbitals that have high densities on either terminus metal atom, as evidenced by orbital coefficients, c_{n1} and c_{n2}. Woitellier *et al.* discuss two criteria for choosing the combination of molecular orbitals, both of which can in some cases lead to different orbital pair choices. The Bloch criterion selects, for a combination of ϕ_1 and ϕ_2, the two molecular orbitals (ψ_n) which have the greatest sum weights on the relevant basis orbitals of the terminus atoms: $c_{n1}^2 + c_{n2}^2$. The Fourier criterion chooses those orbitals for which the modulus of the product weights on the terminus atoms' basis orbitals is the maximum: $|c_{n1}c_{n2}|$.

Considering the distance between the terminus atoms (~10 Å), the electronic overlap of their relevant orbitals [$\langle\phi_1|\phi_2\rangle$] can be neglected, and the ECP for the combination of the nth and mth orbitals can calculated using the following relationship:

$$(ECP)_{nm} = \left| \frac{1}{2} \frac{c_{n1}c_{n2} - c_{m2}c_{m1}}{c_{n1}c_{m2} - c_{n2}c_{m1}} (E_1 - E_2) \right| \tag{2.4}$$

where c_{ij} is the coefficient of the jth terminus atom's relevant orbital within the ith molecular orbital; and E_i is the energy of the ith molecular orbital.

As in Reference [16], semiempirical calculations were used to consider the criteria and calculate ECP for the system as a function of twist angle. Calculations were carried out in Gaussian03 [17] and utilized Extended Hückel Theory for structures minimized at B3LYP using the 6-31G(d,p) basis set for the small atoms and the LANL2DZ basis set and pseudopotential for the Au atoms. For the present system, it is evident that the Au atoms' half-full 6s orbitals and amine groups' lone pairs dominate the Au-N bonds. The system's HOMO and LUMO orbitals were found to satisfy both the Bloch and Fourier criteria for the Au(6s)→Au(6s) channel, and wavefunction weights on these 6s orbitals far exceeded those on the Au atoms' other valence orbitals for any system orbital. Consequently, only the Au(6s)→Au(6s) channel was considered in calculations of the ECP.

2.3 Results

According to the calculations at B3LYP/6-31G(d,p), the lowest energy configurations for biphenyl and 4,4'-diaminobiphenyl molecules in the gas phase have twist angles of approximately 38° and 36°, respectively, showing that the added

amine groups affect the structure slightly. (See Figure 2.3.) The energy calculations showed that the presence of the gold atoms shifted the energy minimum for 4,4'-diaminobiphenyl to 30°. Calculations for biphenyl at MP2/6-31G(d,p) revealed an energy minimum around 45°. Venkataraman *et al.*'s calculations using the PBE functional and 6-31G(d,p) basis with the LACVP** basis for Au yielded angles of 39°, 34°, and 29° at the energy minima for biphenyl, 4,4'-diaminobiphenyl, and 4,4'-diaminobiphenyl with two Au atoms, all within 2° of the values calculated here [7].

Using biphenyl as a reference, the computed minimum twist angles reported here bracket the experimental gas phase values of range 40°–44.4° [18][19]. In a variety of solvents, biphenyl's twist angle is found to decrease, with angles ranging from 19°–37° [19][20][21][22]. There is, then, expected error in using computed twist angle values in the gas-phase for the diaminobiphenyl derivatives in the analysis of the conductance experiment. If the nonpolar solvent used in experiment has a flattening effect on all the derivatives [23], it is likely that the DFT computed values in the gas-phase slightly overestimate the experimental values in solvent. The error could be on order of 10°. However, the presence of the electrodes is shown in the computation here and in Reference [7] to flatten 4,4'-diaminobiphenyl; in the laboratory, the electrodes' effect on the geometry is uncertain.

Furthermore, thermal fluctuations give rise to a range of twist angle values for a given molecule since the rotation barrier is roughly 0.1 eV. A thermal average of 4,4'-diaminobiphenyl was carried out using energy curve results from the B3LYP/6-31G(d,p) calculations. The curve was first fit to a 5th order polynomial, and the average twist angle based on this fit using Boltzmann statistics

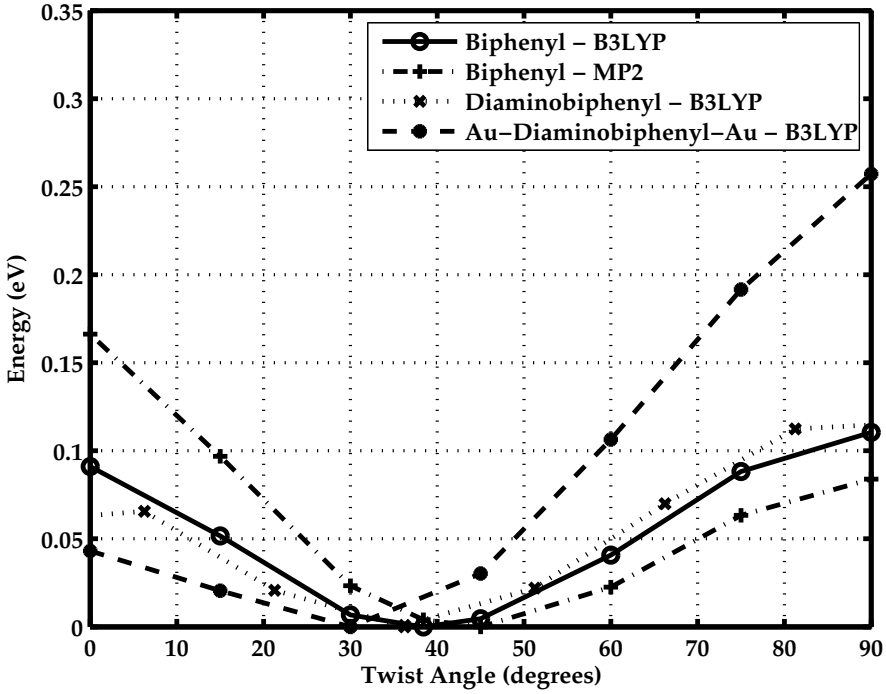

Figure 2.3: Energy curves with respect to twist angle

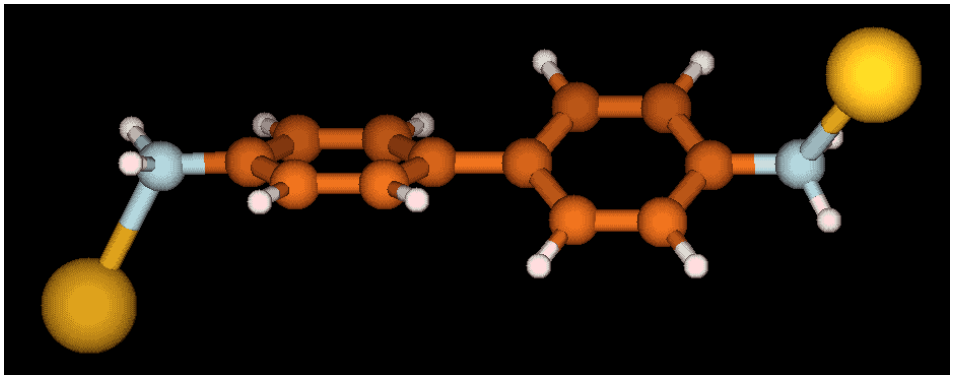

Figure 2.4: Lowest energy state of 4,4′-diaminobiphenyl and two flanking Au atoms calculated using the described DFT methods.

at room temperature was found to be about 4° greater or 3.5° lower than the minimum value at 36°. This is compared to Venkataraman *et al.*'s average value at 1.5° greater than the minimum. Thermal averaging of the tunneling probability showed that the highest probability for charge transfer occurs at 33°, which is 3° less than the minimum energy configuration for 4,4'-diaminobiphenyl and 3° more than the that for 4,4'-diaminobiphenyl with two Au atoms (see Figure 2.5). The energy difference among these configurations is minimal and within the error of computation. This is similar to the referenced work, in which the highest probability of tunneling is at a twist angle 2.5° than the minimum.

Considering the range of values found experimentally for biphenyl alone and the broad histograms generated in this experiment, using calculated twist angles for either diaminobiphenyl derivatives in isolation or with electrodes in the gas-phase seems sufficient. To be consistent, Venkataraman *et al.* chose to use twist angles calculated for 4,4'-diaminobiphenyl in their analysis. Their choice of the seven substituted diaminobiphenyls samples the range of twist angles (from 0° to 90°) so that the overall trend is apparent, despite the error.

These results give information about the most likely configurations of the molecules between the electrodes but tell nothing about whether the majority of the conductance traces were actually recorded at these configurations. In other words, though the complex of electrodes and bridge molecules may be in the energy minimum, a charge transfer may not occur and may be improbable. Missing from Venkataraman *et al.*'s research is computational or theoretical insight linking molecular structure to experimental evidence: they have assumed that the tunneling probability has a particular dependence on the twist angle, in accordance with a system involving qualitatively different electrode-ligand

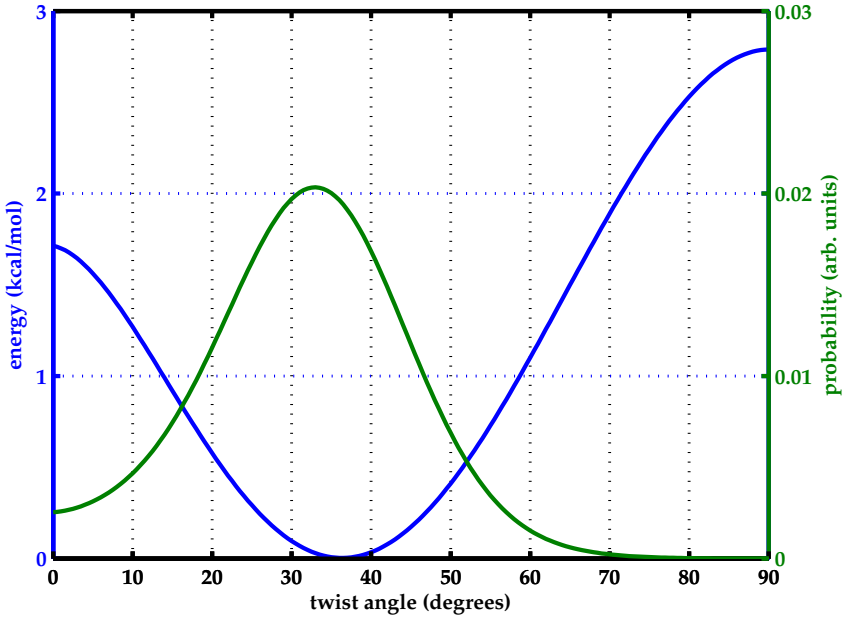

Figure 2.5: Energy surface for 4,4′-diaminobiphenyl (blue) and thermally averaged probability (green)

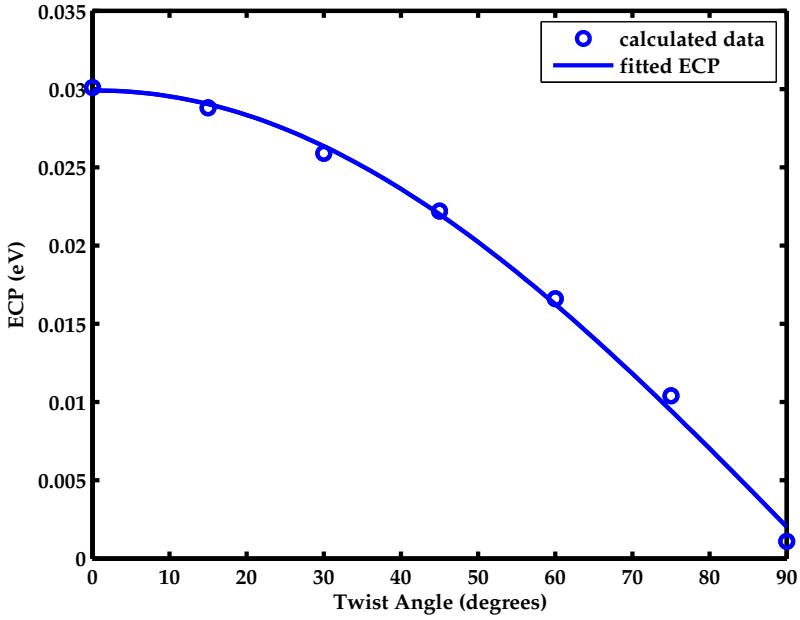

Figure 2.6: Effective coupling parameter for 4,4′-diaminobiphenyl

linkages [16]. One way of connection the molecular structures with measurement is explicitly calculating configuration-specific charge transfer rates with the aid of computational methods.

To measure the relative rates among the different ligand configurations, the effective coupling parameter (ECP), directly related to the resonance integral of Equation 2.2, has been calculated by assuming that the other variables of the rate equation do not measurably vary with twist angle. Examination of the ECP for the dominant conduction channel [Au(6s)→Au(6s)], which transports charge from one electrode to the other, reveals a roughly sinusoidal dependence on the twist angle: data fitted to a general cosine function shows that the ECP goes approximately as $\cos\theta$ (see Figure 2.6). As θ increases to 90°, moving from flat to twisted, the effective coupling between terminus Au atoms monotonically decreases, bringing the value to nearly zero at 90°.

These results show that there is a non-zero probability of charge transfer when the twist angle is less than 90°. Since conduction occurs for virtually the whole range of twist angles and the ground state configuration of the complex of the electrodes and ligands is the most probable, it is reasonable to assume that the ligand molecule has a twist angle near that of the ground state when a conductance trace is recorded. In addition, the results fit appropriately with the experimental results, provided the assumptions used in the method are valid and that side groups in the derivatives used in experiment have a much smaller effect on the molecular energy levels compared to the twisting between phenyl groups. The results are qualitatively identical to that of Reference [16], which dealt with Ru(p) orbitals interacting *directly* with a π-system through nitrogen linkages. In that study, the N of the Ru-N bond was a part of the π-system,

whereas in this case, the Au(s) orbitals are linked to the diaminobiphenyl π-system through an intermediate nitrogen. Despite the added barrier of the nitrogen's lone pair here, the results are still similar to the former system: though the nitrogen atoms' lone pairs dominate the ligand's bonds to gold, it is the HOMO and LUMO orbitals that are primarily responsible for the observed trends. The calculations show that the system's frontier orbitals, which lie in the π-system of the ligand, mediate tunneling and that twisting of the ligand between the two phenyl groups pinches off π-conjugation and, consequently, charge transport, as expected.

2.4 Discussion

While these calculations complemented experiment well, analysis of laboratory methods and bonding interactions between the electrodes and ligands must be considered carefully before applying them to similar systems. The low voltages used in Venkataraman *et al.*'s work placed the molecular wires in a regime for which the ligands' energy levels were the primary modulators of charge transport. If higher voltages are used, molecular vibrations may have a large effect in charge mediation, and different approaches must then be used. The weak bonding between the gold electrodes and amine groups of the 4,4'-diaminobiphenyl allowed for the approximation of the conductance shown in Equation 2.1. A greater extent of bonding (for example, a chemisorbed ligand) would call for other forms of the conductance relationship.

Despite limited knowledge on the exact configuration of the bridging molecules in the device, the energy and ECP calculations make the case that

the central dihedral angles of the 4,4′-diaminobiphenyl derivatives lie within a narrow range of those angles at the energy minima of the relaxed structures during the transfer of an electron from one electrode to the other. The calculations may not go so far as to elucidate the configuration of the ligand at the points of contact with the electrodes, but evidence that the extent of π-conjugation in the molecules is responsible for the differences seen among the set of molecules supports the findings that twist angles obtained from the relaxed structures are those found in experiment.

The differences in metal-ligand bonding between Woitellier's bipyridal system and the diaminobiphenyl system here are not reflected in the ECP trends: it is the aromatic rings that dominate the trends. In the former system, the metals are directly complexed to the π-system, whereas in the latter the gold atoms bond to nitrogen atoms outside of the π-system. Thus, it is likely that for similar ligands, varying the functional groups which make physisorbed contact to the electrodes has a negligible effect on the conductance trends with twist angle: these added barriers do not change the aromatic rings' modulation.

Using electronic structure calculations at the semiempirical level, applied to computed structure of 4,4′-diaminobiphenyl with constrained twist angles is sufficient in reproducing experimental conductance trends in molecular wires of selected derivatives. There is undoubtedly non-negligible error in the magnitudes of ECP from calculation. In general, conductance values can be ballparked through estimation of different parameters [11], and higher-level theory can provide conductances accurate to an order of magnitude, as has been demonstrated for similar molecules [24]. Though the method outlined here provides a useful first look at the effects of configuration for single molecules (or a narrow

group of similar molecules), contrasting single molecule transport across a wide range of organic molecules and operating regimes requires more sophisticated computational, theoretical, and experimental methods [25][26].

CHAPTER 3

HOLE MOBILITIES OF PENTACENE AND OLIGOACENES

Pentacene is part of a class of molecules, the polyacenes, that has been used as a standard for electronic devices incorporating organic materials into their conducting channels. These aromatic molecules are composed of fused benzene rings (see Figure 3.1) and form low-symmetry crystal structures with two molecules per unit cell. Practical application of these and other organic materials remains a challenge for several reasons: Fabricating ordered organic thin films for device use is difficult, as film quality is highly sensitive to environmental and processing conditions. Mobility measurements have been shown to be correlated with a material's disorder, illustrating the importance of manipulating film growth [30]. Organic thin films also degrade with time [31], decreasing function of the devices. In general, many hurdles exist in attaining suitable control over device quality, leading to irreproducible experimental measurements.

The problems encountered in characterizing the mechanisms of transport theoretically shadow the inconsistencies observed in experiment. While similar qualitative trends exist across experimental results, the large variance in quantities makes the definitive assessment of theoretically developed models quite elusive. The challenge can be appreciated by looking deeper into the nature of these materials: Pentacene molecules in a crystal are held together by weak Van der Waals interactions in a herringbone structure that leads to highly anisotropic carrier mobilities. In the operating temperature of interest, room temperature, the mean free path of electrons in the crystal is estimated to be on order of a lattice constant [32][33], in contrast to inorganic solids, in which electrons are rather delocalized. The polarization energy of a charge in the crystal, the en-

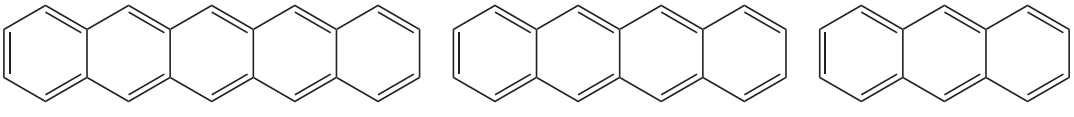

(a) pentacene (b) tetracene (c) anthracene

Figure 3.1: Materials examined in this charge transport study

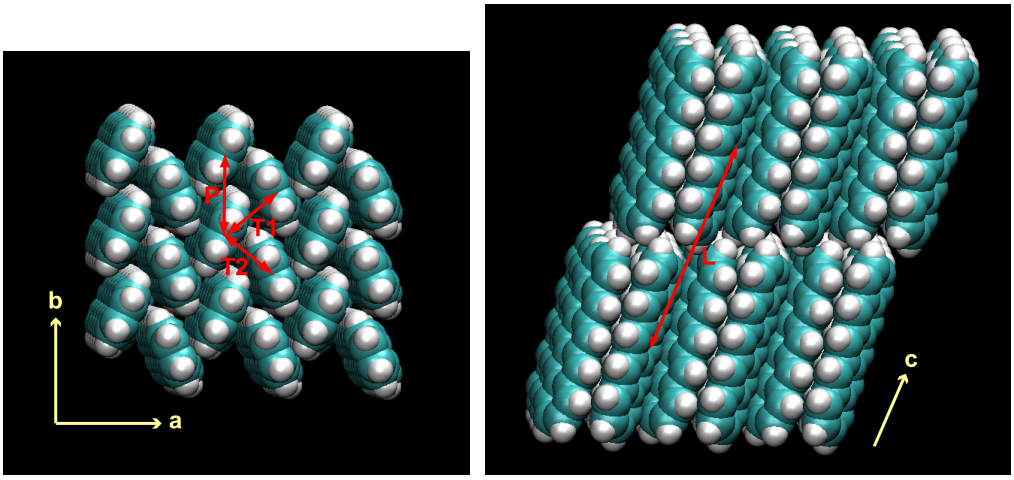

(a) intralayer dimers (b) interlayer dimer

Figure 3.2: Dimers within the pentacene crystal: crystal structures and dimers of the other acenes studied look similar to those of pentacene.

Table 3.1: Experimental oligoacene lattice parameters (adapted from Refs. [27] and [28])

Material	Anthracene	Tetracene	Pentacene
Crystal system	Monoclinic	Triclinic	Triclinic
a (Å)	8.56	7.90	7.90
b (Å)	6.04	6.03	6.06
c (Å)	11.16	13.53	16.01
α (°)	90.0	100.3	101.9
β (°)	124.7	113.2	112.6
γ (°)	90.0	86.3	85.8

ergy decrease associated with the addition of a charge to the crystal, is much greater than the electronic coupling between neighboring molecules[1].

Thus, there is not a high degree of electron delocalization near room temperature, the temperature range of interest for practical use, and the band models often used to employed for inorganic materials do not thoroughly describe the transport characteristics above room temperature for the materials larger than anthracene. In such a temperature range, we expect transport to be dominated by thermally-activated hopping events between single molecule sites, pointing to correlation between local structure and disorder and the movement of charge. However, this picture still fails to accurately describe the transport mechanisms since band mechanisms may still be a factor in combination with hopping mechanisms: after subtracting an extrapolated band contribution to the naphthalene mobility, Karl observed a residual mobility whose logarithm had a nearly linear dependence on the negative inverse of temperature, which is to be expected for pure hopping transport [35]. Some measure of band transport seems to occur in these systems, and the best way to characterize transport in organic molecular crystals and thin films may be a combination of models and mechanisms.

This chapter focuses on the use of computational methods in combination with a classical model to calculate the hole mobilities in crystals of anthracene, tetracene, and pentacene and discusses possible factors controlling charge transport. A review of methods and models used to describe transport are first outlined. The classical mobility model is then introduced, and the result of the calculations presented. The chapter closes with a discussion of the results and how they relate to the picture of transport within the crystals.

[1]The polarization energy for pentacene is calculated to be approximately 1 eV while the electronic coupling is calculated to be on the order of 0.1 eV or lower. See Reference [34].

3.1 Characterization of the Transport Mechanism

As indicated in Reference [35], there are several ways to experimentally measure the charge mobilities of organic materials. The method of measuring charge mobilities most relevant to electronic devices and most commonly used in pentacene mobility studies is field effect transistor experiments. However, difficulties in growing uniform organic layers for transistors and high sensitivity to environmental conditions lead to inconsistent quantitative results. Since theoretical mobility models of organic solids typically make use of idealized static crystal structures, comparison to transistors may not be entirely pertinent. Mobility of the smaller acenes has been measured for single crystals using methods such as the time-of-flight method [36][37], and such measurements lend nicely to interpretation of computational studies and implications of transport behavior in pentacene.

Though low-temperature trends for experimentally determined mobilities of single-crystal naphthalene and anthracene fit the T^{-n} power-law curves typical of band transport, trends in the **c'**-direction show seemingly temperature-independent electron mobilities for T > 100 K, suggesting polaronic-hopping transport, for which charges surrounded by polarization clouds "hop" from one molecular site to another [35][38]. At high temperatures, band transport apparently decreases in prominence as temperature-activated hopping events overtake band transport in efficiency. Pentacene thin-film transistors have shown evidence of hopping transport: near room temperature, hole mobilities increase before reaching a peak and subsequently decreasing [39] above room temperature. An increase in mobility with increasing temperature is consistent with hopping transport, although it should be cautioned that the measured mobility

in Ref. [39] was not corrected for contact resistance, which we expect to also show a strong temperature dependence.

A theoretical understanding of charge transport can be approached by fitting experimental data to proposed models or by developing theoretical models using such constructs as generalized master equations or rate equations. The major problems with the former phenomenological models is that information about the mechanisms of transport is bundled into parameters and that these models can only describe at best a small range of transport behavior. Theoretical models built up from first principles, on the other hand, propose specific mechanisms by which charge is transported through a medium. These models require either estimates or computed values of material properties. Computational methods, such as Monte Carlo simulations [40] and quantum mechanical calculations, are often employed.

The extent of accuracy and the limitations of theoretical models restricts the use of computational methods in the study of charge transport in organic solids. Relevant computational methods have error at or above the energy scales of the quantities of interest, and theoretical models prove to be sensitive to these quantities because of the unique properties of organic materials. Nevertheless, computation can give insight into pieces of the problem that the phenomenological models cannot. There are two main methods of treating the whole crystal system: the first makes use of band models and the second calculates rates of charge transfer between individual molecules.

In the former method, a model Hamiltonian, usually expressed in second quantization formalism, is constructed, and from this, the band structure and other properties are then calculated [41][42]. Quantum mechanical calcula-

tions may be used to estimate the parameters in the Hamiltonian. This method has advantages in that the relative importance of different energy terms in the Hamiltonian (i.e. charge coupling to librational compared to local phonon modes) can be assessed; and several different phenomena may be analyzed through the Hamiltonian, such as temperature dependences and bandwidths. This method, however, assumes band transport, and as has been discussed, other transport mechanisms may be also at play within the crystal. Also, errors in estimation of the Hamiltonian's energy terms invariably lead to error of unknown magnitude in the mobility calculations. While qualitative trends and features may be useful products from this treatment, the method cannot yet provide suitable quantitative estimations.

The second method, in which charge hopping rates between molecules are calculated, generally makes use of the Marcus rate equation (Equation 2.2) or a variation of the golden rule. The rates of charge transfer are connected to the mobility by calculation of a representative diffusion rate, which can be inserted into the Einstein relation for mobility. In contrast to the former method, band transport is ignored. In their assumption of hopping transport and use of highly idealized crystal systems, researchers imply that their calculations can either provide trends across a class of materials [43][29] or limiting behavior [44] with respect to specific properties (e.g. reorganization energies, mobilities). This view may be misguided, however, as errors in computation may either overestimate or underestimate material properties leading to a misinterpretation of trends. The crucial measure of these particular mobility calculations is how they represent trends across materials and with respect to parameters (i.e. temperature) as compared to experimental data.

Here, a study of this approach that combines quantum mechanical calculations with a hopping transport model is presented to assess the viability of these methods for understanding charge transport in the room temperature regime. The model is applied first to three oligoacene materials, from anthracene to pentacene, and then trends in pentacene are examined more thoroughly.

3.2 Mobility Calculations

Following Deng and Goddard's [29] (DG) method, the hole mobilities for pentacene and smaller acenes have been calculated by treating electrical conduction as a series of uncorrelated hops from one molecular site to a neighboring site. The rate of charge transfer between individual molecules is first determined using Marcus' rate equation for transfers between adjacent molecules. Subsequent calculation of a representative diffusion constant for charge diffusion and application of the Einstein relation lead to the materials' carrier mobilities.

The electron transfer reaction can be described the equation, $D+A \rightarrow D^{+}+A^{-}$, where D is the electron donor and A is the electron acceptor, both of which are molecules within the solid. Equation 2.2, used to calculate charge transfer rates, contains two parameters that express energy changes across the reaction coordinate: the free energy change, ΔG°; and the reorganization energy, λ. Here, it is assumed that the free energy change is negligible. The reorganization energy, which represents the energy difference of the system in the product's geometric configuration with and without charge being transfered, can be partitioned into intramolecular and solvent[2] terms, λ_i and λ_o, respectively, so that $\lambda = \lambda_i + \lambda_o$.

[2]Here, and throughout this section, the term "solvent" refers to the solid state environment around the donor and acceptor pair.

The inner-sphere term, λ_i, is exclusive to the molecules between which charge is transferred and includes their vibrational changes. The outer-sphere term, λ_o, references the changes in solvent polarization that need to take place for a charge transfer to occur. In the case of organic molecular crystals, the "solvent" is a solid state medium, and this term implicitly includes the crystal's librational modes. λ_o is neglected, in general, though its magnitude may be on order of λ_i.

Assuming the outer-sphere reorganization energy and free energy change are negligible for an electron transfer event, equation 2.2 reduces to

$$k_j = \frac{2\pi}{\hbar} V_j^2 \left(\frac{1}{4\pi\lambda_i k_B T} \right)^{\frac{1}{2}} \exp\left[-\frac{\lambda_i}{4k_B T} \right] \tag{3.1}$$

for a pair of molecules, j, where $V_j = \left| \left\langle \psi_{f,j} \left| H \right| \psi_{i,j} \right\rangle \right| = \left| \left\langle \psi_{A,j} \left| H \right| \psi_{D,j} \right\rangle \right|$.

The calculation of the inner-sphere reorganization energy, λ_i, can be expressed as the sum of energies relating to the charged and uncharged molecular species in their respective geometries and in the opposite geometries:

$$\lambda_i = (E_D^+ + E_A^-) - (E_D + E_A) \tag{3.2}$$

The subscripts on the energies, E, denote the relaxed geometry of either the donor D or acceptor A. The energies without superscripts are the electronic energies of the ions in their respective geometries. E_D^+ is the energy of the donor with a missing electron; E_A^- is that of the acceptor with an added electron. Here, it is assumed that λ_i is the same for any pair of molecules in the lattice between which charge is transferred, and all energies are calculated for isolated molecules. It is not likely that λ_i would deviate much in the crystal environment from the gas-phase value because of its rigid structure [45]. The local electric fields in the crystal are unlikely to distort the C-C bond lengths in pentacene, relevant since the ring breathing vibrational mode is the dominant mode

in the vibrational reorganization energy calculation. Strong constant, unidirectional electric fields in our DFT calculations shift C-C bond lengths by at most 0.006 Å, 0.4% of the equilibrium bond length with no field. For the strongest applied fields, calculated hole reorganization energies shift by up to 0.008 eV, an insignificant amount when considering the error in these calculations.

For a hole transfer reaction, the electronic coupling, V_j, is approximated as half the energy splitting between the HOMO orbital and the orbital directly below it for the dimer (donor-acceptor complex):

$$V_j = \frac{1}{2}\left(E_{HOMO,j} - E_{HOMO-1,j}\right) \tag{3.3}$$

Within the crystals, each molecule has four unique nearest-neighbor pairs (eight total pairs). V_j is calculated for the isolated dimers, out of the crystal environment. Figure 3.2 shows nearest-neighbor dimers for pentacene, which look similar to those in the crystal structures of anthracene and tetracene.

Once all of the rates have been calculated for transfers between each of the nearest neighbors, the diffusion coefficient is calculated using the following relationship,

$$D = \frac{1}{2n}\sum_j r_j^2 k_j P_j \tag{3.4}$$

where j is the index for a dimer pair; r_j is the distance between neighboring dimers; n is the dimensionality; and P_j is the probability of transfer between molecules of the ith dimer pair relative to all nearest-neighbor dimers. P_j is given by,

$$P_j = \frac{k_j}{\sum_l k_l} \tag{3.5}$$

Once the diffusion coefficient is determined, the carrier mobility is then calcu-

lated using the Einstein relation,

$$\mu = \frac{e}{k_B T} D \tag{3.6}$$

where e is the charge of an electron.

The reorganization energies, λ_i, and the electronic coupling, V_j, were calculated using density functional theory and *ab initio* calculations at the B3LYP and MP2 theory levels, respectively. The configuration of molecules inside the unit cell have been optimized using lattice parameters from literature [27][28] (see Table 3.1) and minimizations with the MM3 potential [46] using the Tinker software package [47]. Mobilities were calculated at $T = 300K$.

3.3 Results

The inner-sphere reorganization energy, λ_i, was calculated for hole transfer in pentacene using various basis sets at the B3LYP and MP2 theory levels. The range of λ_i values corresponding to the number of basis sets used at the B3LYP level is minimal, about 0.02 eV; the shifts in geometry using different optimization methods also do not change the energies appreciably (see Table 3.2). There is an increase of around 0.08 eV from the B3LYP energies to the calculated MP2 energy.

These values are in the range of those published in literature ? both experimentally and computationally determined [29][48]. Gruhn *et al.* [49] have used gas-phase photoelectron spectroscopy to calculate the inner-sphere vibrational reorganization energy of pentacene and have deduced a value of 0.118 eV; their DFT calculations, which expand λ_i as a sum of weighted vibrational frequen-

cies, bracketed their experimental results (ranging from 0.046 eV to 0.178 eV). Thus, the preceding method which utilizes single point rather than vibrational calculations is sufficient in quantitatively estimating the inner-sphere reorganization energy. The low basis set dependence follows Sancho-Garcia's observation [48] about DFT calculations of λ_i for oligoacenes. These results and the lack of experimental data for the electronic coupling parameter led to the choice of B3LYP/6-31G(d)//B3LYP/6-31G(d) and MP2/6-31G(d)//B3LYP/6-31G(d) for the theory levels and basis sets used.[3] This allows for a contrast between a hybrid functional (B3LYP) and Hartree-Fock theory with included electron correlation (MP2).

The inner-sphere reorganization energy is expected to decrease and the electronic coupling to increase with increasing acene size due to the increased number of resonance structures. Putting together these arguments, a positive trend in mobility with chain length is hypothesized. Comparisons of λ_i and V_j for the different molecules and dimers are presented in Tables 3.3 and 3.4. The reorganization energy's downward trend with oligoacene length when using B3LYP/6-31G(d) is not the same result seen in the MP2/6-31G(d) calculations. In the latter, λ_i decreases by about 0.03 eV from anthracene to tetracene and then increases twofold from tetracene to pentacene. The electronic coupling is seen to increase with oligoacene length for the dominant dimers (T1 and T2). The L and P dimers have low coupling values for each material, and a considerable amount of interlayer conduction is not anticipated.

Considering the sensitive dependence of the electron transfer rate on the reorganization energy, it is expected that tetracene will have a relatively large

[3]For the remainder of this section, the theory level and basis set presented will refer to the energy calculation as opposed to the geometry optimization, which will be understood to refer to B3LYP/6-31G(d), unless otherwise noted.

mobility compared to the other two oligoacenes when using MP2/6-31G(d). This is reflected in the mobility results (see Table 3.5). In addition, the MP2/6-31G(d) method predicts that pentacene has a lower hole mobility than that of anthracene. Experimental results on single crystals of these materials show, however, that anthracene (0.4–1.3 cm^2/V-s [50]; 1.0 cm^2/V-s [37]) and tetracene (0.5–0.8 cm^2/V-s [36]) have similar hole mobilities and that pentacene has a higher mobility (3 cm^2/V-s [51]; 8 cm^2/V-s [52]). The calculated mobilities for tetracene using both methods and pentacene at the MP2 level are on order of 10 cm^2/V-s, much higher than experiments to date.

Also troubling are these results compared to those of DG, who used different polymorphs for tetracene and pentacene. Their calculated hole mobilities using B3LYP/6-311G(d,p) are 1.84, 4.24, and 5.37 cm^2/V-s for anthracene, tetracene, and pentacene, respectively, a narrow range ($\approx$ 4 cm^2/V-s). The difference between their mobilities and those reported here at the B3LYP level is related to the slightly variant dimer lengths, electronic coupling, and reorganization energy used, though the bulk of the change is attributed to the electronic coupling, which depends on the dimer configuration and basis set used. Comparing the V_j values for the T1 and T2 dimers (for which the majority of charge transfer occurs) using B3LYP, DG's values are 0.06–0.07 eV less than those reported here for all of the oligoacenes studied. The sensitivity to coupling values, the error in DFT calculations, and the lack of experimental evidence to guide these quantities lead to an uncertainty in how well this method can reflect the physical system.

The mobility trends observed are both quantitatively and qualitatively inconsistent with experiment, for which a clear trend is not immediately appar-

ent. These calculations, which only include hopping transport, also fail to reflect other transport mechanisms, such as band-like transport, and to include other possibly significant contributions to the rate equation, such as vibrational coupling. In the following discussion, corrections to the rate equation and trends in the mobility calculations will be considered for pentacene hole transport in an attempt to gauge the applicability of the method to these crystal systems.

3.4 Discussion

In the mobility calculations, it has been assumed that transport can be described as a series of charge hopping events using a classical Marcus rate equation. An inherent assumption in Marcus' formation of the rate equation is that all relevant vibrational modes are excited. In the context of the crystal systems at room temperature, this assumption may not readily apply to the intramolecular vibrations. Additionally, the treatment leaves out the crystal environment and vibrational effects which may have larger effects on transport than they are credited with. The outer-sphere reorganization energy, one representative quantity for these effects, has been neglected as is common, though its magnitude may be substantial.

The outer-sphere reorganization energy, λ_o, is related to the electronic and vibrational properties of the crystal environment. In practice, it is challenging to calculate a value that incorporates molecular-scale details of the solvent, so a given medium is most often treated as an isotropic dielectric continuum. In Marcus' approximation of λ_o, the acceptor and donor are viewed as spherical bodies within a dielectric continuum with charges at their centers. The approx-

imation is given by [14]:

$$\lambda_\circ = (\Delta e)^2 \left\{ \frac{1}{2a_1} + \frac{1}{2a_2} - \frac{1}{R} \right\} \left\{ \frac{1}{\epsilon_\infty} - \frac{1}{\epsilon_\circ} \right\} \tag{3.7}$$

Here, Δe is the amount of charge transferred; a_1 and a_2 are the radii of the two reactants; R is the distance between the reactants' centers; and ϵ_∞ and $\epsilon_\circ$ are the solvent?s optical and zero frequency dielectric constants, respectively.

In the acene crystals, the assumptions used in Marcus' approximation are rather liberal since charge is spread across a nonspherical molecule, and the polarizability tensor is highly anisotropic [53]. The preceding equation, however, can allow for ballpark estimations to compare the magnitude of λ_o with λ_i. Here, pentacene's outer-sphere reorganization energy is calculated. Taking R to be the center of mass distance between pentacene nearest neighbors in the crystal (as in Figure 3.2) and equating the radii of reactants ($a_1 = a_2$), a_1 and the last factor of the relationship, Q ≡ $1/\epsilon_\infty$ - $1/\epsilon_\circ$, are varied. If ϵ_∞ is taken to be $(1.6)^2$, approximately the square of the refractive index [54], and $\epsilon_\circ = 3$ (Ref. [53]) to be good estimates of the actual values in pentacene, then a value of Q = 0.06 is obtained. Letting $a_1 = R/2$ and this approximate value of Q, electron transfers within the **ab** plane have $\lambda_\circ$ values on the order of 0.1 eV (0.17 eV for the T1 dimer, 0.16 eV for the T2 dimer, and 0.14 for the P dimer). Transfers across pentacene layers have $\lambda_\circ$ values of 0.05 eV (L dimer). Compared to the inner-sphere contribution of roughly 0.1 eV, the intralayer transfers have significant outer-sphere values. In the range considered for the reactant radii and dielectric factor (the preceding estimation of Q was bracketed), $\lambda_\circ$ reached values on order of 1 eV. (See Figures 3.3–3.6.) The range of values is like those estimated for another similar organic medium, phthalocyanine: 0.2–0.5 eV [55]. Thus, the outer-sphere reorganization energy could have a non-negligible effect on the electron transfer rates in the crystal.

Since this outer-sphere contribution is simply added to the total reorganization energy, λ can be treated as an adjustable parameter to study the effect of an addition or correction to the inner-sphere contribution. Figure 3.7 shows the dependence of pentacene's calculated mobility on the total reorganization energy. Near $\lambda = 0.1$ eV, roughly the computed values of λ_i, the slope of the mobility is steep for both computational methods: the mobility decreases by about 3 cm^2/V-s for every 0.01 eV increase in λ. At $\lambda = 0.2$ eV, which corresponds to the sum of estimations for λ_i and $\lambda_\circ$, μ decreases to 3.36 and 4.56 cm^2/V-s for B3LYP/6-31G(d) and MP2/6-31G(d), respectively, closer to experimental values. Here, the change in μ with respect to λ is substantial, though not as high as at $\lambda_i = 0.1$ eV: a decrease of 0.5 and 0.7 cm^2/V-s for a 0.01 eV increase in λ for B3LYP and MP2, respectively.

Despite the fact that more realistic mobility values can be obtained by shifting the value of λ, it should not be forgotten that the electronic coupling is also a quite sensitive parameter, as seen in the comparison to DG's results. Also, as mentioned previously, the assumptions in the classical model for electron transfer may not apply to the system. Equation 2.2 assumes that vibrational energies for modes coupled to the transfer are much smaller than thermal energy so that these modes are all excited: $h\nu \ll k_B T$. In their analysis of the inner-sphere vibrational reorganization energy, Gruhn *et al.* [49] determined experimentally that the dominant modes that coupled to the transfer were to be found at 1347 $\pm$ 33 cm^{-1} (0.17 eV) and 483 $\pm$ 61 cm^{-1} (0.06 eV), the latter an average of low-frequency modes. $k_B T$ at room temperature is 210 cm^{-1} (0.03 eV), so the classical rate equation is not entirely applicable. The following relationship, derived from the golden rule of quantum mechanics, can be used to calculate a rate with

a single coupled vibrational mode [13]:

$$k_{ET} = \frac{2\pi}{\hbar} \left| \left\langle \psi_f \left| H \right| \psi_i \right\rangle \right|^2 \left(\frac{1}{4\pi\lambda_\circ k_B T} \right)^{\frac{1}{2}} (FC) \tag{3.8}$$

$$(FC) = \sum_{v'} \exp(-S) \frac{S^{v'}}{v'!} \exp\left\{ \frac{-(\lambda_\circ + v'h\nu + \Delta G^\circ)^2}{4\lambda_\circ k_B T} \right\} \tag{3.9}$$

Here, the Franck-Condon factor (FC) relates the probability of tunneling between the reactant's $v = 0$ vibrational level and the product's $v = v'$ level for vibration ν. S is the Huang-Rhys factor related to the shift in normal mode coordinates for which the reaction is coupled and can be derived from the intensity of photoelectron spectroscopy bands or computed normal modes. Inspection of the FC reveals that transfers are dominated by transitions in which the outer-sphere reorganization energy and the free energy change cancel the vibrational energy. Any other coupled vibrational modes that can be treated classically can be lumped into $\lambda_\circ$; in this case, a frequency calculated as an average of the low energy frequencies will be added. The effect of vibrational coupling is estimated by using values from Gruhn *et al.*'s work [49]: $S = 0.251$ for the high frequency mode ($\nu = 1347 \pm 33$ cm^{-1}) and $\lambda_1 = 0.017$ eV for the low frequency mode (added to $\lambda_\circ$), as well as a range for outer-sphere reorganization energy and previously used coupling values ($V_j = \left\langle \psi_f \left| H \right| \psi_i \right\rangle$). Downhill reactions will tend to decrease the numerator in the exponential term of FC, so neglecting free energy changes will lead to lower mobilities. Once again, ΔG° will be taken to be 0 and the temperature to be 300 K.

Figure 3.8 shows pentacene hole mobilities calculated using the vibrational correction. λ_1 does not appear to have a substantial impact in the dependence of the mobility, μ, on $\lambda_\circ$, since μ is of such low magnitude. Here, μ is less than those using the classical model by several orders of magnitude. Also, because of the added vibrational energy term in the exponential term of FC, there is a different

dependence on $\lambda_\circ$ from the varying dominance of FC and the prefactor ($\lambda_\circ^{-1/2}$). The mobilities increase with $\lambda_\circ$ until 0.1 eV, from which point they decrease.

The classical model is coarse and implicitly takes into account only some of the many interactions present in the crystal. This semi-classical model, in comparison, has been used to fine-tune the mobility by explicitly including a vibrational contribution. However, a nearly nonexistent mobility is calculated. The vibrational correction could be leading to spurious results because the rate equation sensitively depends on the vibrational modes deemed to have an important role in the electron transfer. It is possible that important vibrational modes were left out, including the environmental low-frequency modes, or that there are other important intramolecular modes within the crystal environment that not immediately obvious. (This argument is not likely as per the discussion of the inner-sphere reorganization energy.) Most of the low-frequency modes can, at room temperature, be treated classically within the outer-sphere reorganization energy term, but they may also play a role in the electronic coupling (V_j) term [56], which is not reflected in the rate equation. The wide disparities in mobility measurements between the two forms of the rate equation convey that calculating mobilities in the preceding manner may be neither accurate nor consistent.

Though this method may not be able to adequately describe the transport mechanisms, it may be useful in the prediction of a material's trends with respect to, for example, temperature and the examination of the relative importance of separate pieces of the puzzle. The latter has been discussed in the section and will continue in the next chapter, in relation to electric fields and impurities affecting transport. A look at the temperature trends implied using

the mobility calculation method will conclude this chapter.

As illustrated by Karl [35], the hopping contribution to naphthalene mobilities are shown to have a nearly linear relationship with $\exp(-A/T)$ from about 100 to 300 K, where A is a positive constant. Single crystal mobility measurements of pentacene using field effect transistors also show similar relationships for the complete hole mobility [57]. Around room temperature, however, researchers observe either a shallow temperature dependence [58] or temperature independence [33]. Minari *et al.* [59] describe a temperature dependence for which the hole mobility increases with increasing temperature with an Arrhenius-like dependence from 45 to 210 K and then slightly *decreases* with increasing temperature. These features are seen in the temperature trends generated from varying the temperature in the mobility calculations (see Figure 3.9): below room temperature, the mobilities increase in an approximately exponential manner with increasing -1/T (corresponding to increasing T) until reaching a maximum at which point the mobilities begin to decrease. This change in trend at the maximum is the result of the temperature dependences found in the prefactor and exponential function of the Marcus rate equation (Equation 3.1) and the Einstein relation (Equation 3.6). Both computational methods (B3LYP and MP2) differ in the placement of the maximum and in the activation energies, E_a (the negative slope of the trend line's linear portion): for B3LYP/6-31G(d), the maximum occurs around 150 K, and E_a is 0.55 meV; and MP2/6-31G(d) has a maximum at 300 K and an E_a of 25 meV. These temperatures bracket that of Reference [59], but the activation energy for B3LYP falls out of the rather large range of reported experimental values (O[1–10 meV]).

Table 3.2: Inner-sphere reorganization energy, λ_i, in eV – Pentacene

Method	λ_i
B3LYP/6-31G(d)//B3LYP/6-31G(d)	0.080
B3LYP/6-31G(d,p)//B3LYP/6-31G(d)	0.093
B3LYP/6-31+G(d)//B3LYP/6-31G(d)	0.092
B3LYP/6-31+G(d,p)//B3LYP/6-31G(d)	0.092
B3LYP/6-311+G(d,p)//B3LYP/6-31G(d)	0.093
B3LYP/6-311+G(2d,p)//B3LYP/6-31G(d)	0.092
B3LYP/6-311+G(2df,2p)//B3LYP/6-31G(d)	0.092
B3LYP/6-311++G(3df,2pd)//B3LYP/6-31G(d)	0.092
B3LYP/6-31G(d,p)//B3LYP/6-31G(d,p)	0.088
B3LYP/6-311G(d,p)//B3LYP/6-311G(d,p)	0.105
MP2/6-31G(d)//B3LYP/6-31G(d)	0.184

Table 3.3: Inner-sphere reorganization energy, λ_i, in eV – Oligoacenes

Material	B3LYP/6-31G(d)	MP2/6-31G(d)
Anthracene	0.13	0.12
Tetracene	0.11	0.09
Pentacene	0.08	0.18

Table 3.4: Electronic coupling in, V_j, in eV – Oligoacenes

B3LYP/6-31G(d)				
Material	V_{T1}	V_{T2}	V_P	V_L
Anthracene	0.16	0.16	3.81 x 10^{-2}	1.36 x 10^{-4}
Tetracene	0.20	0.18	1.41 x 10^{-2}	2.72 x 10^{-4}
Pentacene	0.21	0.19	5.44 x 10^{-4}	2.72 x 10^{-4}
MP2/6-31G(d)				
Material	V_{T1}	V_{T2}	V_P	V_L
Anthracene	0.17	0.17	2.72 x 10^{-4}	2.72 x 10^{-4}
Tetracene	0.23	0.20	2.72 x 10^{-4}	2.72 x 10^{-4}
Pentacene	0.24	0.22	2.72 x 10^{-4}	2.72 x 10^{-4}

Table 3.5: Hole mobilities, in $cm^2/V\text{-}s$ – Oligoacenes

Material	B3LYP/6-31G(d)	MP2/6-31G(d)
Anthracene	4.85	6.87
Tetracene	10.20	16.34
Pentacene	15.56	5.57

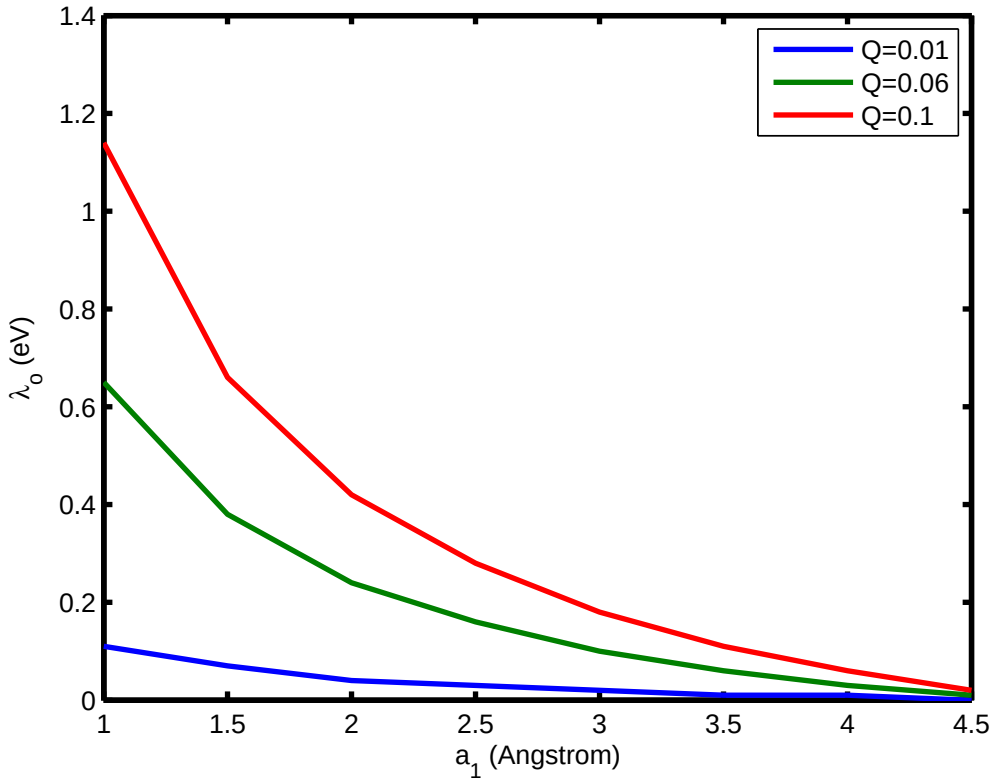

Figure 3.3: Outer-sphere reorganization energy approximations for T1 dimer of pentacene using Marcus' relationship. Q = 0.06 represents an estimation of the actual factor.

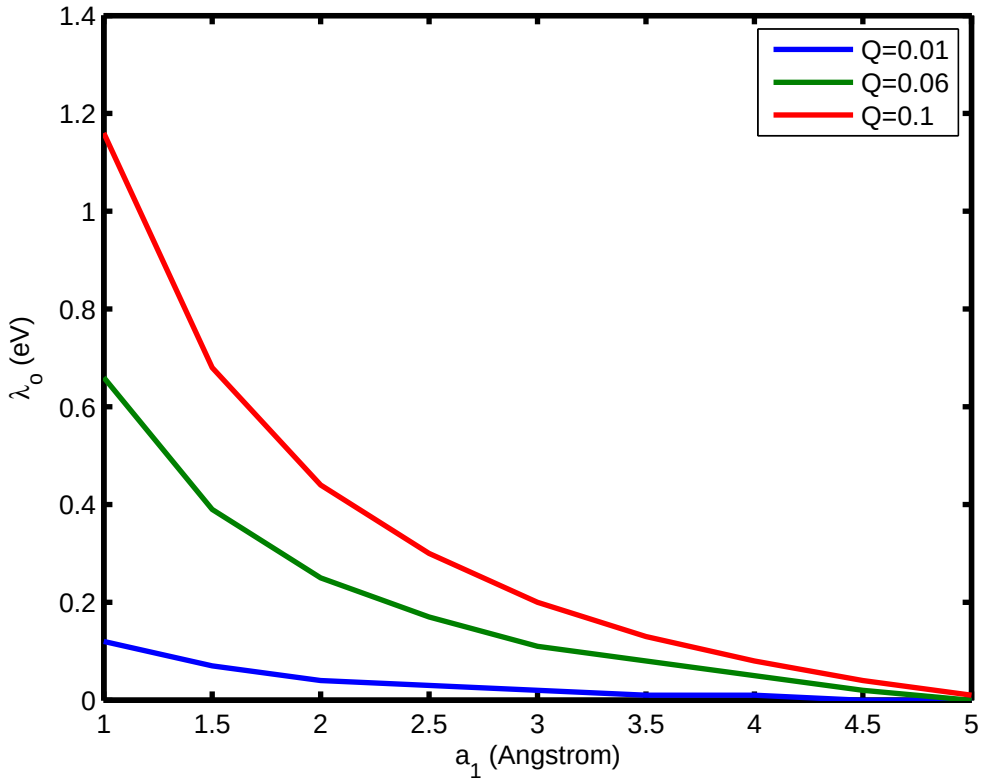

Figure 3.4: Outer-sphere reorganization energy approximations for T2 dimer of pentacene using Marcus' relationship. Q = 0.06 represents an estimation of the actual factor.

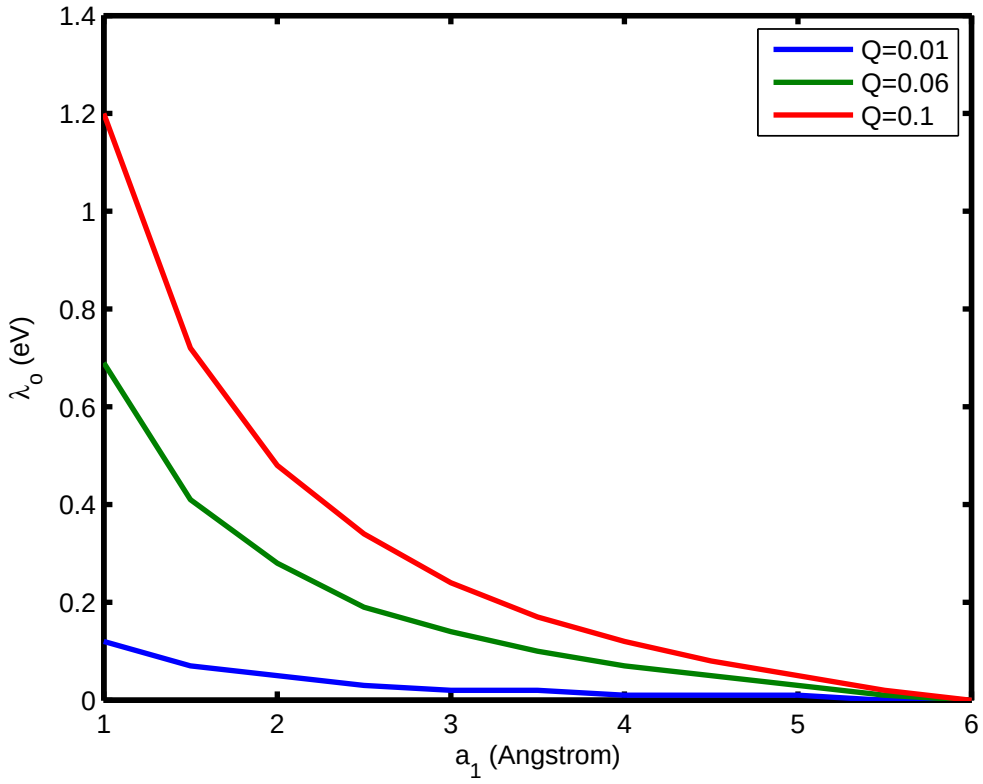

Figure 3.5: Outer-sphere reorganization energy approximations for P dimer of pentacene using Marcus' relationship. Q = 0.06 represents an estimation of the actual factor.

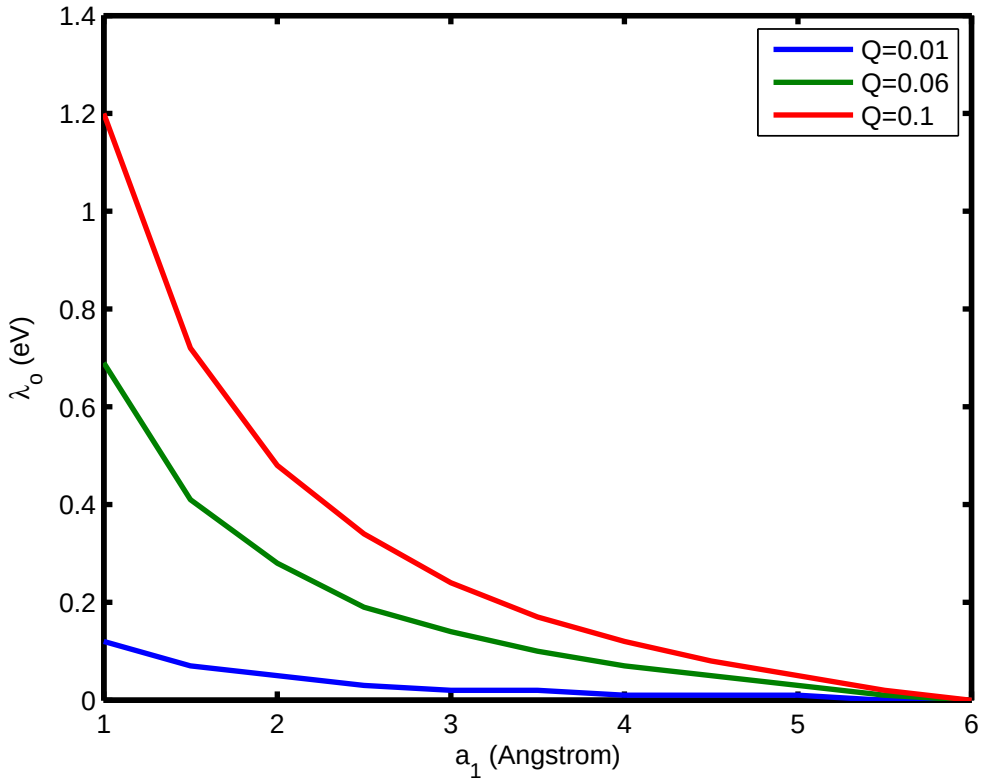

Figure 3.6: Outer-sphere reorganization energy approximations for L dimer of pentacene using Marcus' relationship. Q = 0.06 represents an estimation of the actual factor.

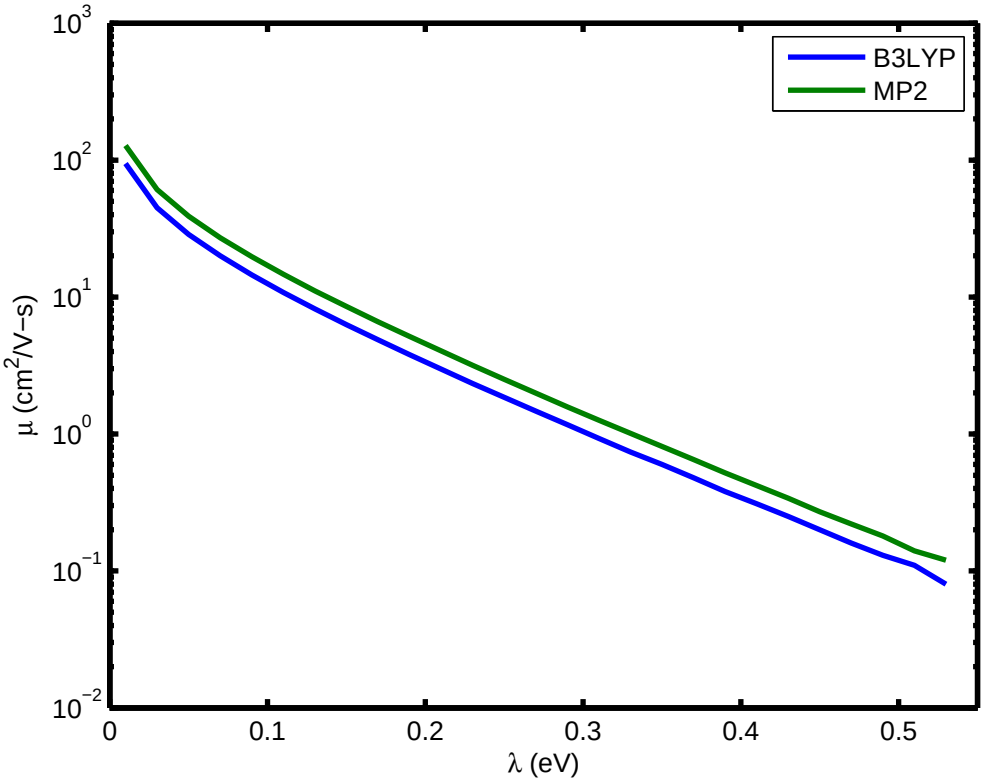

Figure 3.7: Hole mobility of pentacene as a function of the total reorganization energy, λ, using DG's method [29].

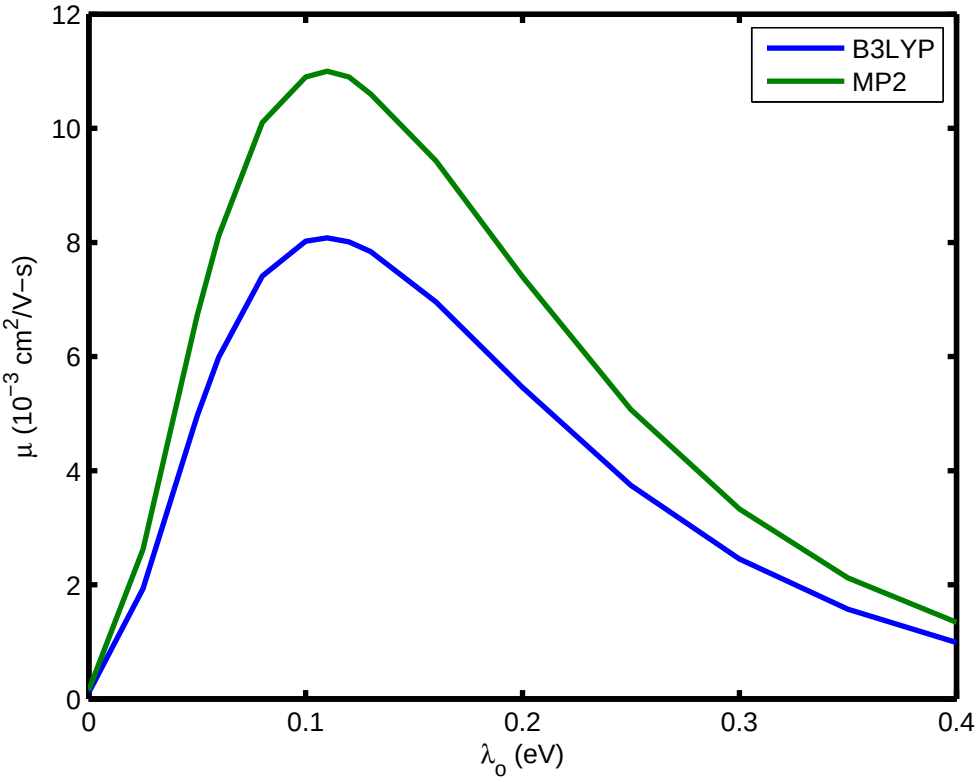

Figure 3.8: Pentacene hole mobility using vibronic form of electron transfer rate (Equation 3.8).

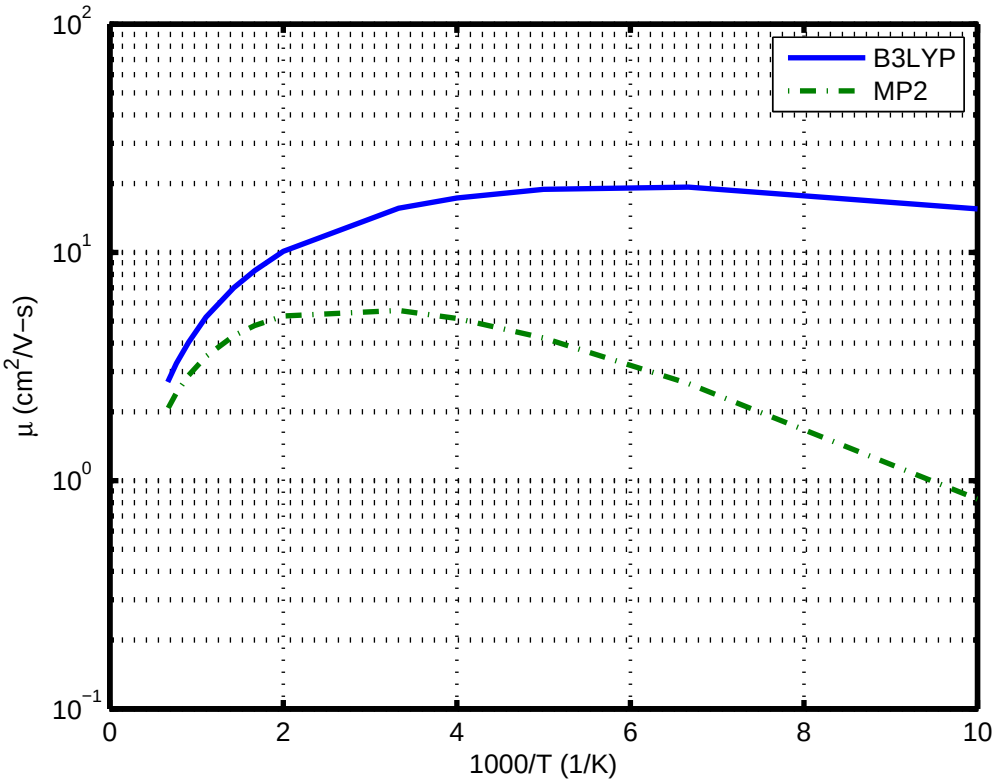

Figure 3.9: Temperature dependence of pentacene hole mobility

The general shape of the calculated trend lines and their temperatures at maximum are promising results (qualitatively) that lend support to the view of transport as being a collection of hopping events, despite the quantitative inconsistencies. The rate equation is, however, a simplistic interpretation of charge transport with multiple factors that depend on temperature. The electronic coupling, for example, varies with the crystal's intermolecular vibrations, which change the relative orientation of the dimers. At room temperature, the probability that these low-frequency modes are excited is non-negligible. This problem has been approached computationally without explicit calculation of librational modes: Troisi and Orlandi use molecular dynamics in combination with semiempirical calculations to quantify the change in coupling values with temperature and find that above 100 K, the standard deviation of coupling values for interlayer dimer pairs is on order of the mean values [60]. In a similar study on pentacene derivatives, Troisi, Orlandi, and Anthony had concluded that low-frequency phonon modes coupled to V_j cannot be merely treated as a perturbation [56].

In short, the abstractions of this semi-classical method coupled with the errors of calculation and general experimental irreproducibility can lead to gross miscalculation of a material's mobility. The method's outputs cannot be seen as suitable estimates for organic molecular crystal mobilities, especially when the description of charge transport is not yet well-formed. This calls into question the utility of comparing results across different materials. The study of temperature trends showed some indication that the method can be used as a starting point in using computational methods to understand specific characteristics of transport in these systems. The main contributions that this and similar applications can provide is a way of studying separate parts of a model's framework, as

researchers have done [60][61]. There are several effects at play in a crystal, not to mention environmental factors, that need to be examined in more detail. Before computation can provide quantitatively accurate numbers and before more descriptive theories can be established, computation can offer a means of probing the complex system and perhaps rules of thumb with regard to selection of new materials.

CHAPTER 4

WATER AND PENTACENE VACANCY DEFECTS

It has been commonly observed that pentacene-based devices degrade with time, and it is posited that the cause of this problem is water and oxygen from the surroundings [31]. Encapsulation of the organic layer in a pentacene thin film transistor has been shown to mitigate mobility decreases compared to exposed devices after a number of days [62][63], and coating substrates with hydrophobic materials has been demonstrated to yield higher carrier mobilities [64][65]. Water vapors, in addition, have been proposed as a cause of hysteresis in organic field effect transistors [66] and lowered saturation currents [67][68]. While the interaction of ambient vapors with pentacene thin films is not well understood, intercalation of oxygen molecules within pentacene crystals and placement of water molecules between layers [69] as well as chemical defects resulting from reactions with water and oxygen [70] have been proposed as possible defects leading to charge trapping states. Kinetics studies of polycrystalline pentacene using electric force microscopy have implied that chemical reactions are a source of charge traps within the crystals [71], lending support for the proposal of traps at chemical defects within the crystal. Experimental reflectivity measurements have implied that several Angstroms of water exists between pentacene and an SiO_2 substrate [72]. Thus, water may have an important implications for crystal structure and device function.

Preliminary molecular dynamics simulations show that water molecules do not penetrate into a pentacene crystal free of defects. If ambient water does indeed have an effect on device performance, molecules must either enter the system through defects and other features (i.e. grain boundaries) or during crystal

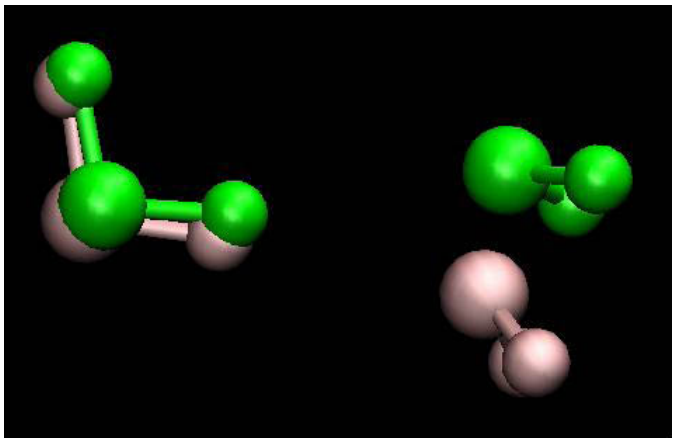

Figure 4.1: Calculated minimum water dimer structures overlaid: MP2/6-31+G(d,p) in pink and MM3 potential in green

Table 4.1: Root mean squared displacements for molecules neighboring vacancy defects in 5×5×2 systems.

(a) Single defect

Number	rms Displacement (pm)
1	64.9
41	28.8
8	19.0
18	61.3
11	33.5
10	9.8

(b) Double defect

Number	rms Displacement (pm)
2	108.8
9	162.2
10	63.3
12	25.4
19	8.4
39	57.6
40	86.5
42	87.0

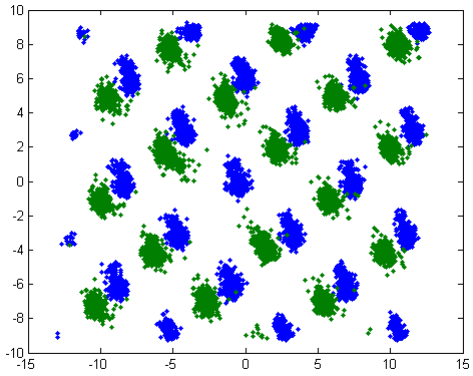

(a) 3×3×2

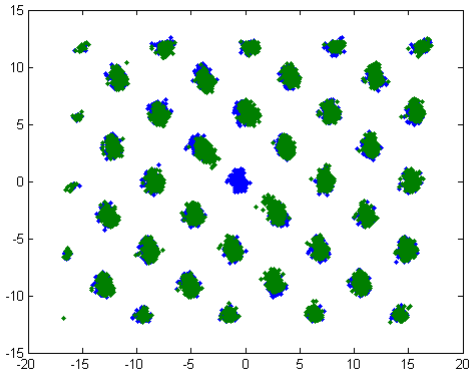

(b) 4×4×2

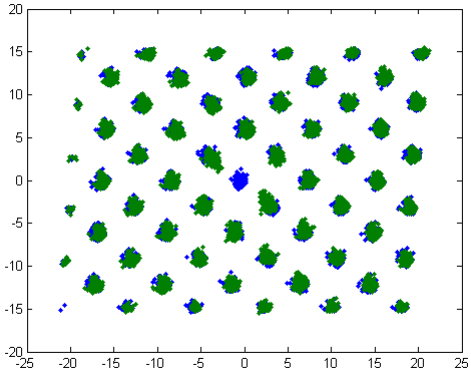

(c) 5×5×2

Figure 4.2: Center of mass plots at different system sizes: single vacancy simulation data (green) overlaid onto baseline simulation data (blue). Coordinates are in Å.

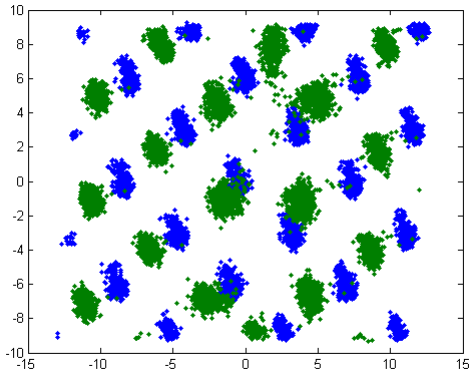

(a) 3×3×2

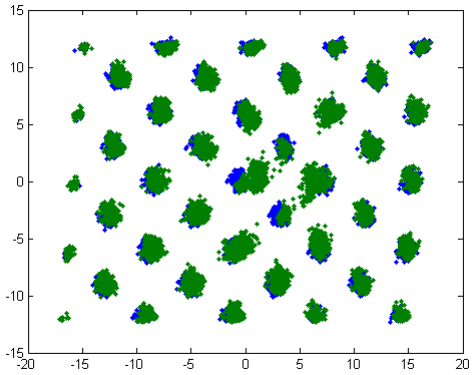

(b) 4×4×2

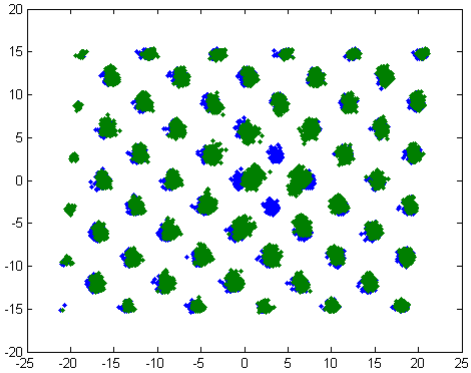

(c) 5×5×2

Figure 4.3: Center of mass plots at different system sizes: double vacancy simulation data (green) overlaid onto baseline simulation data (blue). Coordinates are in Å.

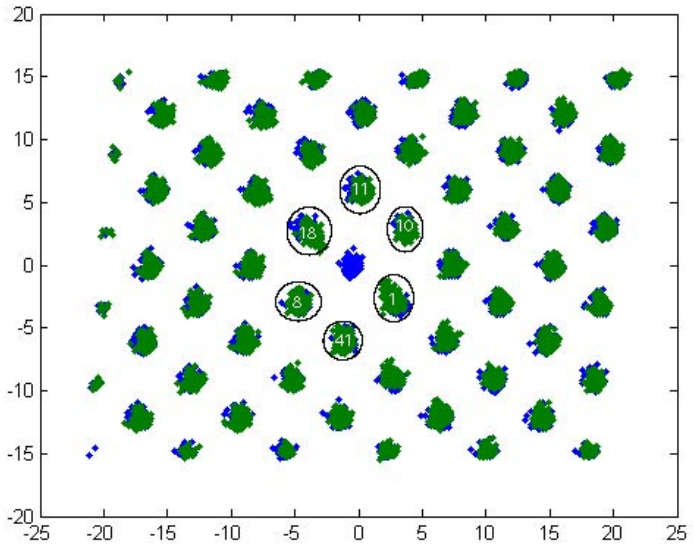

(a) single defect

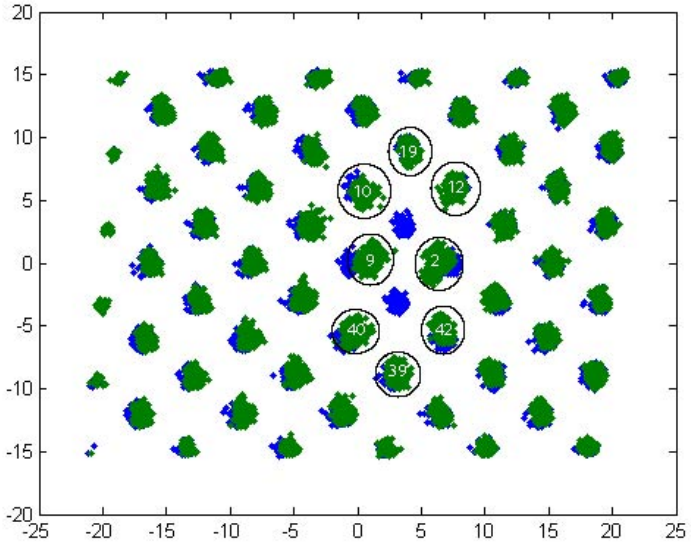

(b) double defect

Figure 4.4: Map of molecules neighboring defects using center of mass plots at the 5×5×2 system size: vacancy simulation data with no impurities (green) overlaid onto baseline simulation data (blue). Coordinates are in Å. Only the double defect systems with argon and two water molecules showed non-negligible differences compared to the control data, primarily for molecules #2, #9, and #40.

Table 4.2: Tilt angles for pentacene molecules neighboring vacancy defects in 5×5×2 systems.

(a) Single defect

Number	Baseline (°)	Single Defect (°)
1	72.5	71.7
41	71.2	71.4
8	72.5	72.2
18	72.2	71.1
11	71.2	70.6
10	72.1	72.4

(b) Double defect

Number	Baseline (°)	Double Defect (°)
2	71.0	64.2
9	71.2	59.3
10	71.2	68.8
12	71.1	67.4
19	72.3	70.1
39	72.4	69.4
40	71.2	63.5
42	71.2	68.8

formation. Vacancy defects, in particular, may play a role in the presence of water in the systems since these defects may be present in significant numbers. An estimate derived through molecular dynamics simulations [74] places the equilibrium concentration of vacancy defects in pentacene crystals to be on order of 10^{13} cm^{-3} at room temperature (one defect per 10^7 unit cells). Experiments on monolayer pentacene [73] yield much higher concentrations of defects, possibly due to kinetics during monolayer growth: 10^{19} cm^{-3} at room temperature (one defect per 10^2 unit cells). Given these magnitudes, chemical impurities which may insert into the vacancies may be the cause of the interesting behavior seen in devices.

In this section, the effect of water impurities on vacancy defects in the pentacene surface is considered, and the consequences concerning charge transport are predicted. The structure of vacancy defects is first studied and followed by a discussion of chemical impurities in the context of defects. Rationalization of related device phenomenon concludes.

4.1 Method and Computation

Molecular dynamics (MD) simulations of a double layer of pentacene with and without vacancy defects and impurities were completed. A double layer was used to simulate the pentacene surface, as an empty volume above the surface was included in the system box. Molecular dynamics simulations were carried out using the molecular mechanics MM3 potential [46] in an NVT ensemble at T=298 K. Simulations were implemented using the Tinker software package [47]. The MM3 potential was chosen because of its suitability to organic molecular crystal structure [75]. Applicability to the system with water and pentacene

was determined by comparing the calculated minimum structures for the water dimer using DFT and the MM3 potential: these two structures are very similar (see Figure 4.1).

The effect of increasing the system size for the double-layer system (n×n×2, where n is an integer and numbers represent multiples of unit cells) was examined. The system size was chosen by considering the convergence in crystal dynamics of systems with induced vacancies as the layers increased in area: a system size that adequately screens the image of the defects across the periodic boundary conditions was necessary. Systems with a single vacancy (one pentacene molecule removed) and a double vacancy (two adjacent molecules removed) were compared against baseline simulations with the same volume of molecular space.

To study the effect of system size, the center of mass locations and tilt angles with respect to the horizontal (**ab**-plane) of the molecules were compared against corresponding molecules in the baseline measurements. Defect formation energies calculated using the minimized structures (at T=0 K) did not show a strong correlation to the system sizes but allowed for rationalization of defect types. Single and double vacancies were created in what will be referred to as the "upper" layer of the pentacene double layer system. The x and y center of mass coordinates for all time points and molecules in the upper layer were plotted in comparison to the baseline calculation (no defects). A correction based on the average z-coordinate of the center of mass was added to align layers across calculations, since added vacuum to the system box could have shifted the whole block of molecules along the **c**-direction. These plots provide a visual representation of the regions in which molecules move. The center

of mass deviations with respect to average locations of corresponding baseline molecules were analyzed. In particular, displacements for molecules adjacent to defects were considered. Tilt angles were studied to find out if the size of the system made a difference in angle ranges and mean values. Tilt angles of the molecules neighboring vacancy defects could be important in examining the effect of chemical impurities (water and noble gases) on structure.

Systems sizes for these preliminary simulations were 3×3×2, 4×4×2, and 5×5×2, with number representing integers of unit cells composed of two pentacene molecules. An additional volume of vacuum three unit cells in length was placed above the bilayer so that the total size of the system box was m×m×5, with m being an integer. The "top" surface of the double layer, in which vacancies were induced, is equivalent to the $(00\bar{1})$ surface. Simulations were run for 10^6 steps with a time step of 0.5 fs, and structural data was collected at 1 ps intervals.

Plots showing the centers of mass for each top-layer pentacene molecule in the systems are shown in Figures 4.2–4.3. Positions for every time recorded are plotted to show the range of molecular movement: each dot represents a center of mass at a time point, and each defined region indicates the space of one molecule. In some cases, a set of regions may represent just one molecule due to a molecule's movement. All plots include data from the baseline simulations to compare against. Well-defined regions are a feature of the baseline simulations (all shown in blue). The 3×3×2 plots with vacancies show marked shifts in center of mass locations with respect to the baseline. In addition, it is apparent that the defects in the double vacancy system drift during the course of the simulation. Increasing the system size to 4×4×2 shows more expected results:

spatial regions for each molecule more closely match the baseline's regions. In the single vacancy data, the vacancy for each system size does not appear to drift. However, the two vacancies in the third simulation appear to wander, since extra and smaller regions of dots appear.

The 5×5×2 data illustrates an apparent convergence: in the double vacancy simulation, the vacancies remain stable and centered at one location. The single vacancy plot looks similar to that of the 4×4×2 simulation but with centers of mass areas that even more closely match the baseline. The plot for the double vacancy shows that the most stable configuration for the defect is one in which two parallel, adjacent pentacene molecules are removed (separated by a **b**-vector). For the whole of the simulation, neither of the two vacancies moves to another location. A similar simulation whose minimized configuration began with a vacancy of one unit cell shifted very soon to and remained in the parallel configuration through the remainder of the simulation. Thus, only this double vacancy configuration will be considered.

The average root mean squared (rms) distance of each center of mass with respect to its average value was measured to determine how bound a molecule is to a particular location. Average rms values shifted from 0.65 to 0.88 Å across all the simulations; for each system size, the average rms distance increased with the addition of vacancies. Average rms distances did not vary widely (within hundredths of an Å) across the system sizes for a given amount of vacancies. Thus, while the center of mass plots show deviations of the vacancy simulation data with respect to control data in terms of overall molecular movement across different system sizes, the rms data show that system size has little effect on the wandering of a molecule from its average location. Molecules adjacent to the

vacancy are another matter, and analysis of geometric changes near a vacancy will be limited to the system size chosen for impurity studies.

Average tilt angles for each molecule were determined using the data from each simulation. For each system size, the average tilt angles for whole systems ranged about 3° from the baseline calculation to the double defect system: baseline tilt angles were on average 72°, and double defect tilt angles were on average 68°. An increase in system size led to near convergence of average tilt angles for the single defect systems, with angles averaging 72° for the 5×5×2 system size, just as in the baseline calculations. It is apparent that two neighboring vacancy defects structurally deform the system much more than one vacancy does.

The 5×5×2 system size was chosen based on visual inspection of the center of mass plots, described previously, and on the near convergence of tilt angle values. The average center of mass locations for molecules neighboring the vacancies were compared to corresponding molecules in the baseline calculations to obtain displacements. Results for the single vacancy simulation were compared to results from Seo *et al.*'s experimental study of pentacene vacancies [73], which used scanning tunneling microscopy. Displacements for the single vacancy simulation range from roughly 10–65 pm, many of which lie within range of Seo *et al.*'s results. (See Figures 4.4 and 4.5; and Chart 4.1.) Two out of the six molecules fall out of range, and the sixth molecule has a displacement that is an order of magnitude smaller than that of Seo *et al.*'s study. For the double vacancy, several displacements are understandably much higher than the range seen in the single vacancy. Two of the smaller displacements lie in the same row (along a **b**-vector) as the vacancies. In general, the molecular dynamics simula-

tions show that these displacements range from 1–100 pm with most on order of 10 pm. This agrees well with the experimental results in Seo *et al.*'s paper.

Tilt angles for molecules neighboring vacancies were also specifically examined for the 5×5×2 system size. (see Table 4.2.) Angles for the single defect simulation do not deviate much from those of the baseline simulation. The double defect simulation shows a different result: molecules neighboring the vacancies can have average angles that deviate greatly from those of the baseline. Differentials range from 2° to 12° degrees. The following calculations that involve chemical impurities can shed light on whether these impurities increase structural order in these systems, and tilt angles can be analyzed as part of the evidence.

The defect formation energy for the surface vacancies was calculated for all the system sizes following the relationship:

$$E_v = E_d - \frac{n - v}{n} E_p \tag{4.1}$$

where E_v is the defect formation energy; E_d is the system energy with the defect; E_p is the system energy of the perfect crystal (no defects); n is the number of molecules in the perfect crystal; and v is the number of vacancy defects (here, 1 or 2). Single defect formation energies for the three system sizes studied were all within a narrow range: 1.3±0.01 eV. These values are slightly less than Drummy *et al.*'s calculated values [74] of 1.7±0.15 eV for interior vacancies using the Dreiding force field and a range of system sizes (from 64 to 288 molecules). Double defect formation energies similarly had little effect from the system size with values of 2.2±0.01 eV, which is less than twice the formation energy for the single surface vacancy. Because a double vacancy represents a smaller formation energy than two separated, single vacancies, double vacancies, which have not

been widely observed or studied, are likely to appear in crystals based on thermodynamic arguments. More computation and analysis is necessary, however, to make such an argument more conclusive.

Water molecules and an argon atom were used as chemical impurities in the chosen 5×5×2 system. Argon, which has a negligible attraction to pentacene, was used as a control to compare to a water molecule's effect on the system. In contrast, one water molecule and a pentacene molecule have a binding energy of up to 0.25 eV according to the MM3 potential. Attraction between an isolated pentacene molecule and water molecule depends on the orientation of the molecules. Up to two water molecules were added to a given system: A calculation of water density for room temperature air saturated with water (T = 298 K, P_{sat} = 3.2 kPa) yields only 0.04 water molecules for the vacuum volume used in simulation. Thus, the presence of only one water molecule in the system would be plausible. As in the system size studies, molecular dynamics simulations were run using an NVT ensemble and MM3 potential with a time step of 0.5 fs, and structural data was collected every 1 ps. The length of the simulations varied depending on the length of insertion events, but all simulations were run for at least 10^6 steps (0.5 ns). The effect of a chemical impurity on the pentacene system was determined by measuring the length of time an impurity remained in a vacancy defect and by studying the same features examined for the system size studies. An impurity was deemed to be inserted into the vacancy defect by the qualification that its z-coordinate was between the boundaries of the pentacene layer in which vacancies lie. For water, the coordinates of the oxygen atom were used to determine the z-coordinate of the molecule.

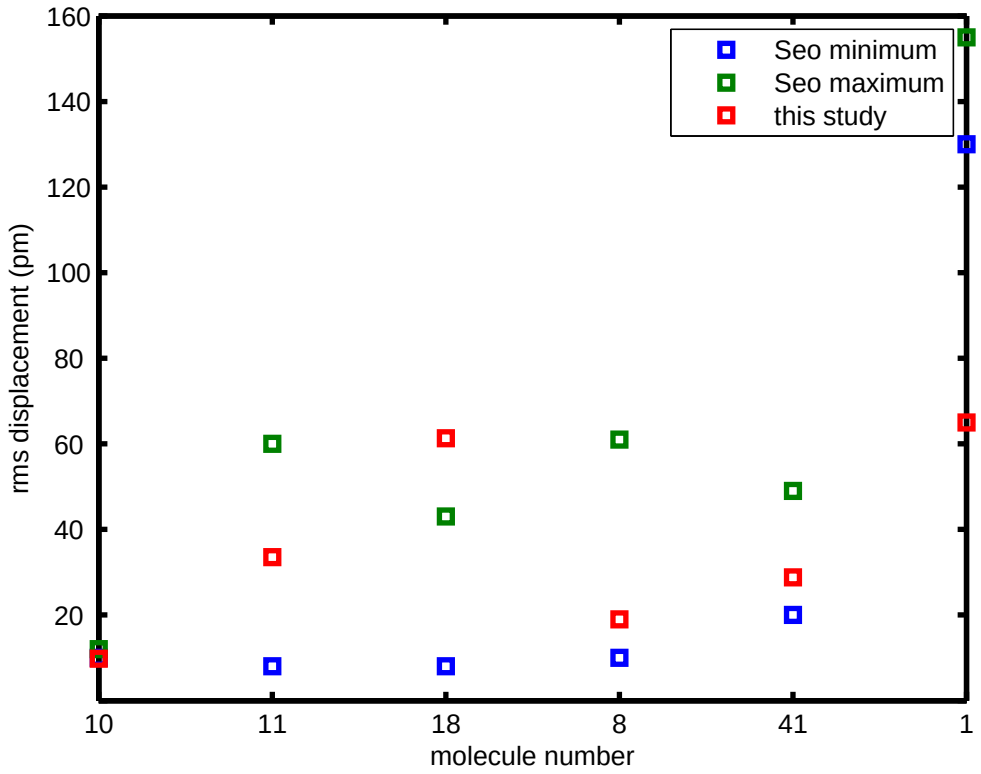

Figure 4.5: Root mean squared (rms) displacements of pentacene molecules neighboring defects: comparison to experimental data from Ref. [73].

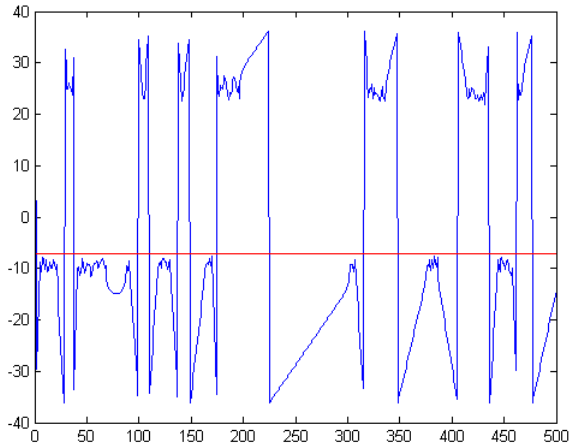

(a) Single argon atom

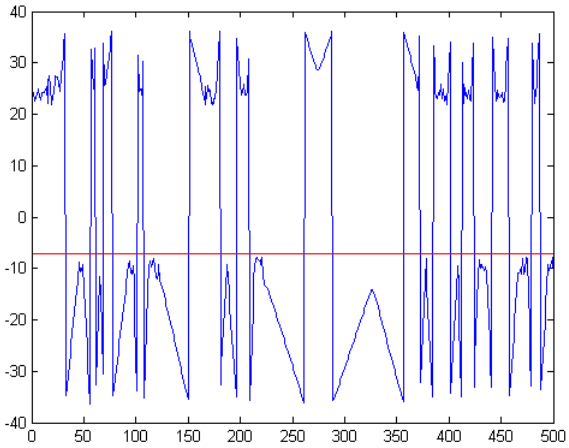

(b) Single water molecule

Figure 4.6: Impurity's z-coordinate as a function of time for control data: line represents "upper" surface of pentacene crystal. Units are in Å and ps. By system definition, impurities enter the vacancies from the negative direction.

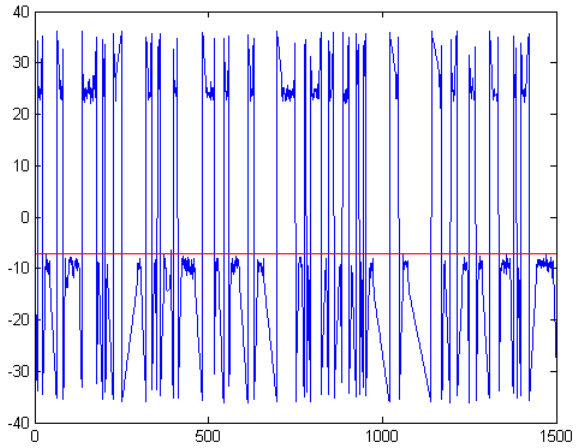

(a) Single argon atom

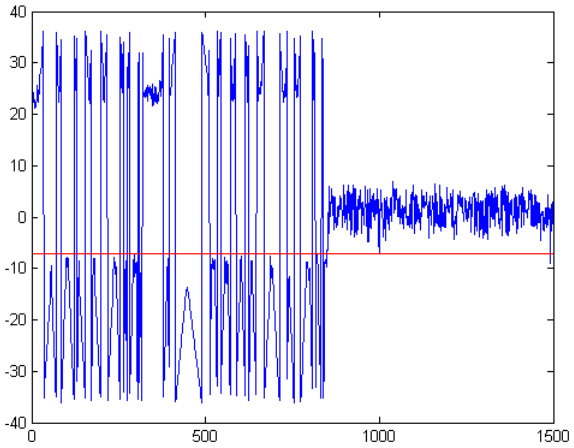

(b) Single water molecule

Figure 4.7: Impurity's z-coordinate as a function of time for single defect and single impurity data: line represents "upper" surface of pentacene crystal. Units are in Å and ps. By system definition, impurities enter the vacancies from the negative direction.

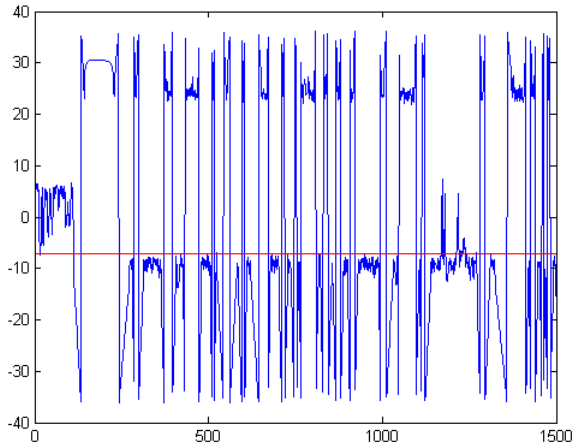

(a) Single argon atom

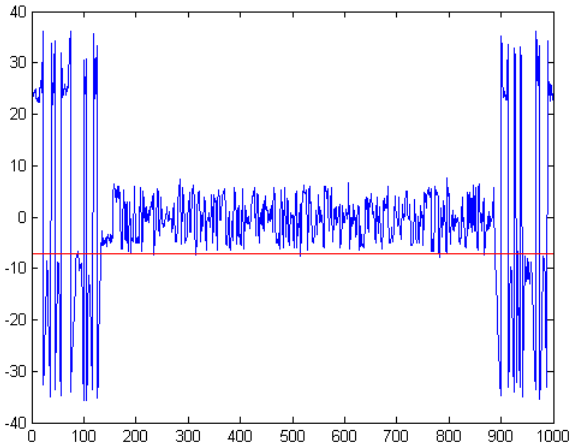

(b) Single water molecule

Figure 4.8: Impurity's z-coordinate as a function of time for double defect and single impurity data: line represents "upper" surface of pentacene crystal. Units are in Å and ps. By system definition, impurities enter the vacancies from the negative direction.

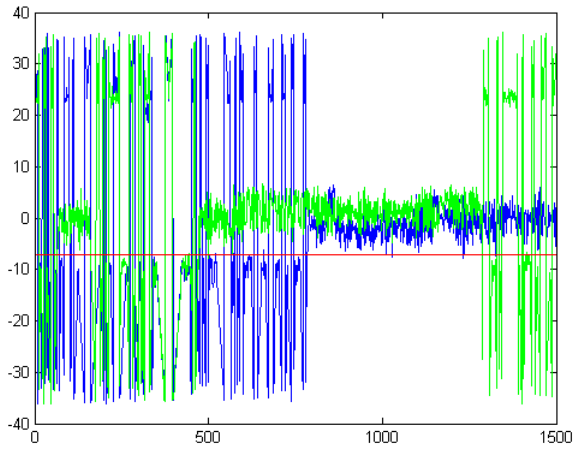

(a) Single defect

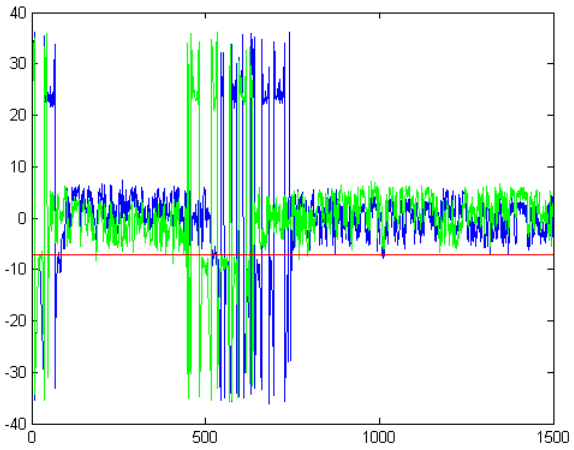

(b) Double defect

Figure 4.9: Impurity's z-coordinate as a function of time for two water molecule data: line represents "upper" surface of pentacene crystal. Units are in Å and ps. By system definition, impurities enter the vacancies from the negative direction.

Table 4.3: Residence times of impurities in vacancy defects. ("+" indicates an indefinite length of residency in a vacancy.)

(a) Single defect

Impurity type	Time (ps)
Argon	–
Water (one)	322
Water (two)	252 (overlap): (i) 358+; (ii) 252

(b) Double defect

Impurity type	Time (ps)
Argon	55
Water (one)	378
Water (two)	(a) 180 (overlap): (i) 219; (ii) 198 (b) 376+ (overlap); (i) 376+; (ii) 430+

4.2 Results

Out of the eight impurity systems studied, only double defect systems showed apparent changes in defect deformation during insertion events. Substantial residence times for insertions (on order of picoseconds) have an uncertain correlation with either the number of impurities or the size of the vacancy: more simulations sampled at longer run times would be needed to make conclusions about average residence times. Notably, argon atoms did not spend a great amount of time within vacancies, and only in the double vacancy system did an insertion actually occur. An argon atom's Van der Waals diameter is roughly 3.7 Å, compared to a water molecule's diameter of approximately 3.2 Å. The difference in behavior between water molecules and argon atoms despite the small differential in diameters can be attributed to the bonding interactions between pentacene and the impurities: pentacene has a weak attraction to water but a negligible interaction with argon. Thus, the crystal vibrations make an argon atom's insertion unfavorable.

As expected, the impurities did not penetrate the control system (no defects). The graphs in Figure 4.6 show that both argon and water molecules bounce off the pentacene surface. In similar graphs representing defect data, then, it is apparent that insertions occur at vacancy defect sites. When a single defect is present, water molecules insert into the crystal, but argon does not. For double defects, insertions occurred for both water systems and the argon system. (See Figures 4.7–4.9.) In most cases, the simulations ran for a window of time in which an impurity inserted into and then released from a vacancy. However, due to time constraints, some simulations were not run long enough. The longest time a water molecule resided in a defect was (at least) 430 ps for one

out of two water molecules in a double defect system. Chart 4.3 summarizes residence times for impurity plus defect systems. It is possible, under favorable conditions, that impurities could remain in vacancies for an indefinite period. While it is obvious that the residence times of water in the defects are considerably longer than that of argon, firm conclusions about the effect of defect size and the number of water molecule impurities cannot be made. What can be concluded is that ambient water molecules are likely to enter surface vacancies and remain for some period of time, here recorded to be at least on order of hundreds of picoseconds. This may be long enough for yet more atmospheric water molecules to enter the defect. Water molecules already present in a defect provide additional bonding interactions with which to attract an extra molecule. Preliminary simulations have shown that the presence of several water molecules in a single defect is a stable system.

Defect deformation in response to the presence of impurities within the vacancies was studied by analyzing center of mass plots, center of mass deviations, and average tilt angles of pentacene molecules. For systems with two water impurities, only data for the period of time in which two molecules resided in the vacancy were used. Compared to control data from like systems with induced defects but no impurities, only the double defect systems with argon and two water molecules showed significant changes and only for three particular molecules adjacent to defects. Pentacene molecule #9 (refer to Figure 4.4(b)) shows substantial movement beyond normal placement in the argon system and in one of the insertions for the two water molecule system. Molecules #2 and #40 shift by 3-5° to be, on average, more upright than counterparts in the control. This shifts them closer to the angles for a system without defects. Average root mean squared distances for center of mass did not shift greatly,

apart from molecule #9 in the argon and one of the water insertions: this pentacene molecule appears to migrate to a neighboring vacancy when an impurity is present, leading to average rms center of mass displacements of 1.93 Å and 1.77 Å, respectively, compared to the control's value of 0.93 Å. Thus, the presence of impurities can cause vacancy defect migration, at least for a double defect, in what would be an otherwise stable system.

In contrast to Tsetseris *et al.* [69], the presence of water molecules between pentacene layers does not appear to be favorable for water entering the system from atmosphere, as no instances of water migrating between layers occurs in the simulations presented here. In their study, a binding energy of 0.55 eV for an intact water molecule between two pentacene layers was calculated using plane-wave DFT. This calculation does not take into account the kinetics of the system, however. Even if there theoretically exists such a binding interaction, its formation from atmospheric water molecules would be unlikely: water does not appear to bind to either the $(00\bar{1})$ or the (001) surfaces of pentacene, implying that water would not remain there during crystal growth. Additionally, Tsetseris *et al.* found metastable configurations in which water molecules reside within an otherwise defect-free pentacene layer at the expense of neighboring pentacene molecules' rigidity. As discussed, the MD simulations here do not show insertion of water molecules from the atmosphere into perfect crystals. It should be mentioned that this study does not cover the possible uptake of water molecules from a wetted underlying substrate. Impurities from a layer of water on a substrate such as SiO_2, present before pentacene deposition, could conceivably migrate during or after crystal formation to develop structures similar to those determined by Tsetseris *et al.* Further studies must be carried out to understand the dynamics of such a configuration and the relative energies

between competing structures.

4.3 Discussion

It has been shown that water molecules do enter surface vacancy defects in pentacene and can remain within the defect for periods on order of hundreds of ps. The change in residence time due to the presence of two molecules as opposed to a single molecule is unclear from the studies of single and double vacancy defects. Argon atoms, which have Van der Waals radii only tenths of Angstroms more than that of water molecules, remain in double defect systems for an order of magnitude less than that of water and, in these studies, were not shown to enter single defects at all. Thus, water's insertion into and residence within the defects must be due to its bonding interaction with pentacene.

These simulations, while demonstrating insertions, cannot fully describe the average behavior of such systems. Further studies would need to be carried out. The data collected do suggest that water molecules can reside within defects for at least hundreds of picoseconds and that the residence time is long enough for a second molecule to insert. Consequently, vacancy defects may fill with several water molecules. Preliminary simulations suggest that several water molecules can reside in single and double vacancies for a non-negligible amount of time.

The added impurities did not appear to affect significantly the defect structure. In addition, none of the impurities migrated throughout the pentacene crystal – all remained within vacancies. Inert gases such as argon have not been shown to affect charge transport in pentacene, as expected, but humid air has a measurable effect on devices [76]. Jurchescu *et al.* have suggested from ex-

perimental data that water from the atmosphere can diffuse through pentacene single crystals, leading to a decrease in saturation current [68]; and Goldmann *et al.* report trap formation in pentacene single crystal devices exposed to humid air on timescales consistent with diffusion of small molecules through organic molecular crystals [65]. The former reference attributes added trapping due to absorbed water molecules within the crystal whereas the latter suggests water layers accumulate at the interface of the substrate, causing discrete trap energy level.

The simulations here show that water molecules only enter the pentacene crystal through surface vacancies and do not move throughout the crystal, but this does not preclude the possibility of water molecules diffusing through crystal defects, grain boundaries, and device interfaces. This research implies that water molecules can occupy vacancy defects in pentacene, and thus, experimental observations of pentacene field effect devices in humid air may be the result of water molecules populating such structures or other structural defects in the crystals as proposed by Zhu *et al* [76]. Further computational studies to determine the likelihood of water molecules residing between pentacene and various substrates and within other disordered structures are needed to compare the significance of such occurrences with the impurities found in vacancy defects.

If water is present in organic devices exposed to ambient air, the remaining question is how the impurities affect charge transport. Water molecules within the crystal may affect charge transport by inducing energetic disorder through charge-dipole interactions and thereby creating trap states [76][77][78]. Gap states related to chemical impurities formed from reactions between wa-

ter and pentacene have also been proposed [70]. Study of chemical reactions within the crystal was beyond the scope of this study, but the results presented here are a starting point for such investigation. Future computational studies could probe the possibility of chemical reactions of pentacene with water and the electronic structure changes due to the presence of chemical impurities.

CHAPTER 5

CONCLUSION

This report on organic electronic systems has proceeded from a static description of tunneling in a single molecule system to a dynamic study of chemical impurities in a larger organic molecular crystal. Electronic structure calculations using density functional theory and semiempirical methods were used to demonstrate the physical basis of the tunneling's dependence on the twist angle of 4,4'-diaminobiphenyl. A method of calculating the hole mobility based on classical electron transfer theory of pentacene crystals was analyzed using *ab initio* and density functional calculations. This method was found to be inadequate in predicting mobilities and sensitive to the calculated parameters. Molecular dynamics simulations were utilized to consider the possible effects of chemical impurities, specifically water, on pentacene vacancy defects. Water molecules were found to insert into surface defects and remain for a period of time that likely allows for additional molecules to enter, which has implications for charge transport.

These studies illustrate that understanding the physical basis of charge transport in such devices requires a detailed knowledge of complex electronic processes within the charge conducting medium. Each study has shown that the relevant energy scales for organic materials fall within the error of the particular computational methods employed herein. In addition, these energy scales may cause the systems to be sensitive to environmental factors, such as thermal fluctuations and energetic disorder from impurities or structural imperfections. Higher level computation may provide more accurate results but may be impractical depending on resource and time constraints. Also, while theory of

single molecule transport may be sufficient to allow for more advanced computation to predict experimental results, the theory of larger systems, as in organic molecular crystals, is not well-developed enough due to the systems' several non-negligible dynamic processes [79] and the difficulty in connecting theory to often irreproducible experimental results.

If the purpose of computation is to screen candidate organic materials for devices, serious challenges hinder its usage. Ideally, efforts would include prediction of a material's structure and electronic properties solely from simulation, but both of these are complicated problems. Computation, however, can prove useful in identifying potential factors affecting transport and guiding researchers in the control of devices; computation may reveal effects not able to be observed through experimental means. In this study, for example, water molecules were shown to bind to vacancy defects in pentacene crystals through MD simulations. These results are a step toward rationalizing existence of the pentacene gap states proposed by Northrup and Chabinyc [70], which require reaction with impurities such as water and oxygen. In addition, they support Jaquith, Muller, and Marohn's hypothesis that trapping in polycrystalline pentacene originates from chemical reactions of pentacene cations at structural defect sites [71]. Though further simulations are needed to show how reactions leading to trapping states may take place within a crystal, the study presented here shows how computation can provide a link between theory and experiment. Thus, despite its limits, computation has an important role to play in the analysis of transport in organic materials.

BIBLIOGRAPHY

[1] P. M. Borsenberger and D. S. Weiss, *Organic Photoreceptors for Xerography*. Boca Raton, FL: Taylor & Francis, 1998.

[2] A. Aviram and M. A. Ratner, "Molecular rectifiers," *Chem. Phys. Let.*, vol. 29, no. 2, pp. 277–283, 1974.

[3] H. Koezuka, A. Tsumura, and T. Ando, "Field-effect transistor with polythiophene thin film," *Synth. Met.*, vol. 18, pp. 699–704, 1987.

[4] E. A. Silinsh and V. Capek, *Organic Molecular Crystals: interaction, localization, and transport phenomena*. New York: AIP Press, 1994.

[5] C. P. Collier, E. W. Wong, M. Belohradsky, F. M. Raymo, J. F. Stoddart, P. J. Keukes, R. S. Williams, and J. R. Heath, "Electronically configurable molecular-based logic gates," *Science*, vol. 285, pp. 391–394, 1999.

[6] J. Locklin and Z. Bao, "Effect of morphology on organic thin film transistor sensors," *Anal. Bioanal. Chem.*, vol. 384, pp. 336–342, 2006.

[7] L. Venkataraman, J. E. Klare, C. Nuckolls, M. S. Hybertsen, and M. L. Steigerwald, "Dependence of single-molecule junction conductance on molecular conformation," *Nature*, vol. 442, pp. 904–907, 2006.

[8] A. Troisi and M. A. Ratner, "Molecular signatures in the transport properties of molecular wire junctions: What makes a junction 'molecular'?," *Small*, vol. 2, no. 2, pp. 172–181, 2006.

[9] A. Troisi, J. M. Beebe, L. B. Picraux, R. D. van Zee, D. R. Stewart, M. A. Ratner, and J. G. Kushmerick, "Tracing electronic pathways in molecules by using inelastic tunneling spectroscopy," *Proc. Nat. Acad. Sci.*, vol. 104, no. 36, pp. 14255–14259, 2007.

[10] L. Venkataraman, J. E. Klare, I. W. Tam, C. Nuckolls, M. S. Hybertsen, and M. L. Steigerwald, "Single-molecule circuits with well-defined molecular conductance," *Nano Let.*, vol. 6, pp. 458–462, 2006.

[11] A. Nitzan, "A relationship between electron-transfer rates and molecular conduction," *J. Phys. Chem. A*, vol. 105, pp. 2677–2679, 2001.

[12] A. Nitzan and M. A. Ratner, "Electron transport in molecular wire junctions," *Science*, vol. 300, pp. 1384–1389, 2003.

[13] P. F. Barbara, T. J. Meyer, and M. A. Ratner, "Contemporary issues in electron transfer research," *J. Phys. Chem.*, vol. 100, pp. 13148–13168, 1996.

[14] R. A. Marcus, "On the theory of oxidation-reduction reactions involving electron transfer. I," *J. Chem. Phys.*, vol. 24, no. 5, pp. 966–978, 1956.

[15] A. Nitzan, "Electron transmission through molecules and molecular interfaces," *Annu. Rev. Phys. Chem.*, vol. 52, pp. 681–750, 2001.

[16] S. Woitellier, J. P. Launay, and C. Joachim, "The possibility of molecular switching: Theoretical study of $[(NH_3)_5Ru\text{-}4,4'\text{-}bipy\text{-}Ru(NH_3)_5]^{5+}$," *Chem. Phys.*, vol. 131, pp. 481–488, 1989.

[17] M. J. Frisch, G. W. Trucks, H. B. Schlegel, G. E. Scuseria, M. A. Robb, J. R. Cheeseman, J. A. Montgomery, Jr., T. Vreven, K. N. Kudin, J. C. Burant, J. M. Millam, S. S. Iyengar, J. Tomasi, V. Barone, B. Mennucci, M. Cossi, G. Scalmani, N. Rega, G. A. Petersson, H. Nakatsuji, M. Hada, M. Ehara, K. Toyota, R. Fukuda, J. Hasegawa, M. Ishida, T. Nakajima, Y. Honda, O. Kitao, H. Nakai, M. Klene, X. Li, J. E. Knox, H. P. Hratchian, J. B. Cross, C. Adamo, J. Jaramillo, R. Gomperts, R. E. Stratmann, O. Yazyev, A. J. Austin, R. Cammi, C. Pomelli, J. W. Ochterski, P. Y. Ayala, K. Morokuma, G. A. Voth, P. Salvador, J. J. Dannenberg, V. G. Zakrzewski, S. Dapprich, A. D. Daniels, M. C. Strain, O. Farkas, D. K. Malick, A. D. Rabuck, K. Raghavachari, J. B. Foresman, J. V. Ortiz, Q. Cui, A. G. Baboul, S. Clifford, J. Cioslowski, B. B. Stefanov, G. Liu, A. Liashenko, P. Piskorz, I. Komaromi, R. L. Martin, D. J. Fox, T. Keith, M. A. Al-Laham, C. Y. Peng, A. Nanayakkara, M. Challacombe, P. M. W. Gill, B. Johnson, W. Chen, M. W. Wong, C. Gonzalez, and J. A. Pople, *Gaussian03, Revision C.02*. Wallingford, CT: Gaussian, Inc., 2004.

[18] A. Almenningen, O. Bastiansen, and L. Fernholt, "Structure and barrier of internal rotation of biphenyl derivative in the gaseous state," *J. Mol. Struct.*, vol. 128, pp. 59–76, 1985.

[19] H. Suzuki, "Relations between electronic absorption spectra and spatial configurations of conjugated systems. I. Biphenyl," *Chem. Soc. Jap.*, vol. 32, no. 12, pp. 1340–1350, 1959.

[20] M. Akiyama, T. Watanabe, and M. Kakihana, "Internal rotation of biphenyl

in solution studied by IR and NMR spectra," *J. Phys. Chem.*, vol. 90, pp. 1752–1755, 1986.

[21] A. d'Annibale, L. Lunazzi, A. Boicelli, and D. Macciantelli, "The conformational problem of biphenyl in solution as investigated by the liquid crystal nuclear magnetic resonance spectrum of 3,3',5,5'-tetrachlorobiphenyl," *J. Chem. Soc. Perkin Trans. 2*, pp. 1396–1400, 1973.

[22] V. J. Eaton and D. Steele, "Dihedral angle of biphenyl in solution and the molecular force field," *J. Chem. Soc. Faraday Trans. 2*, vol. 69, pp. 1601–1608, 1973.

[23] M. Kato, M. Higashi, and Y. Taniguchi, "Effect of pressure on the internal rotation angle of biphenyl in carbon disulfide," *J. Chem. Phys.*, vol. 89, no. 9, pp. 5417–5421, 1988.

[24] M. P. Samanta, W. Tian, S. Datta, J. I. Henderson, and C. P. Kubiak, "Electronic conduction through organic molecules," *Phys. Rev. B*, vol. 53, no. 12, pp. R7626–R7629, 1996.

[25] A. W. Ghosh and S. Datta, "Molecular conduction: Paradigms and possibilities," *J. Comp. Elec.*, vol. 1, pp. 515–525, 2002.

[26] A. Troisi, M. A. Ratner, and A. Nitzan, "Vibronic effects in off-resonant molecular wire conduction," *J. Chem. Phys.*, vol. 118, no. 13, pp. 6072–6082, 2003.

[27] R. B. Campbell and J. M. Robertson, "The crystal structure of hexacene, and a revision of the crystallographic data for tetracene and pentacene," *Acta Cryst.*, vol. 15, pp. 289–290, 1962.

[28] R. B. Campbell, J. M. Robertson, and J. Trotter, "The crystal and molecular structure of pentacene," *Acta Cryst.*, vol. 14, pp. 705–711, 1961.

[29] W.-Q. Deng and W. A. Goddard III, "Predictions of hole mobilities in oligoacene organic semiconductors from quantum mechanical calculations," *J. Phys. Chem. B*, vol. 108, pp. 8614–8621, 2004.

[30] T. Ji, S. Jung, and V. K. Varadan, "On the correlation of postannealing induced phase transition in pentacene with carrier transport," *Org. Elec.*, vol. 9, pp. 895–898, 2008.

[31] C. Pannemann, T. Diekmann, and U. Hilleringmann, "Degradation of organic field-effect transistors made of pentacene," *Mat. Res. Soc.*, vol. 19, no. 7, pp. 1999–2002, 2004.

[32] V. M. Kenkre, "Finite-bandwidth calculations for charge carrier mobility in organic crystals," *Phys. Let. A*, vol. 305, pp. 443–447, 2002.

[33] J. Takeya, C. Goldmann, S. Haas, K. P. Pernstich, B. Ketterer, and B. Batlogg, "Field-induced charge transport at the suface of pentacene single crystals: A method to study charge dynamics of two-dimensional electron systems in organic crystals," *J. Appl. Phys.*, vol. 94, pp. 5800–5804, 2003.

[34] E. V. Tsiper and Z. G. Soos, "Charge redistribution and polarization energy of organic molecular crystals," *Phys. Rev. B*, vol. 64, p. 195124, 2001.

[35] N. Karl, "Charge carrier transport in organic semiconductors," *Synth. Met.*, vol. 133–134, pp. 649–657, 2003.

[36] R. W. I. de Boer, M. Jochemsen, T. M. Klapwijk, A. F. Morpurgo, J. Niemax, A. K. Tripathi, and J. Pflaum, "Space charge limited transport and time of flight measurements in tetracene single crystals: A comparative study," *J. Appl. Phys.*, vol. 95, pp. 1196–1202, 2004.

[37] N. Karl, J. Marktanner, R. Stehle, and W. Warta, "High-field saturation of charge carrier drift velocities in ultrapurified organic photoconductors," *Synth. Met.*, vol. 41–43, pp. 2473–2481, 1991.

[38] M. Pope, "Electronic processes in organic solids," *Ann. Rev. Phys. Chem.*, vol. 35, pp. 613–655, 1984.

[39] M. Zhu, G. Liang, T. Cui, and K. Varahramyan, "Temperature and field dependent mobility in pentacene-based thin film transistors," *Sol. St. Elec.*, vol. 49, pp. 884–888, 2005.

[40] H. Bässler, "Charge transport in disordered organic photoconductors," *Phys. Stat. Sol. B*, vol. 175, pp. 15–56, 1993.

[41] K. Hannewald and P. A. Bobbert, "Anisotropy effects in phonon-assisted charge-carrier transport in organic molecular crystals," *Phys. Rev. B*, vol. 69, p. 075212, 2004.

[42] K. Hannewald, V. M. Stojanovic, J. M. T. Schellekens, and P. A. Bobbert,

"Theory of polaron bandwidth narrowing in organic molecular crystals," *Phys. Rev. B*, vol. 69, p. 075211, 2004.

[43] V. Coropceanu, O. Kwon, B. Wex, B. R. Kaafarani, N. E. Gruhn, J. C. Durivage, D. C. Neckers, and J.-L. Brédas, "Vibronic coupling in organic semiconductors: The case of fused polycyclic benzenethiophene structures," *Chem. Eur. J.*, vol. 12, pp. 2073–2080, 2006.

[44] G. R. Hutchison, M. A. Ratner, and T. J. Marks, "Hopping transport in conductive heterocyclic oligomers: Reorganization energies and substituent effects," *J. Amer. Chem. Soc.*, vol. 127, pp. 2339–2350, 2005.

[45] S. T. Bromley, F. Illas, and M. Mas-Torrent, "Dependence of charge transfer reorganization energy on carrier," *Phys. Chem. Chem. Phys.*, vol. 10, pp. 121–127, 2008.

[46] N. L. Allinger, Y. H. Yuh, and J.-H. Lii, "Molecular mechanics. the MM3 force field for hydrocarbons. 1," *J. Am. Chem. Soc.*, vol. 111, no. 23, pp. 8551–8566, 1989.

[47] J. W. Ponder, *Tinker, Version 4.2*. 2004.

[48] J. C. Sancho-Garcia, "Assessment of density-functional models for organic molecular semiconductors: The role of Hartree-Fock exchange in charge-transfer processes," *Chem. Phys.*, vol. 331, pp. 321–331, 2007.

[49] N. E. Gruhn, D. A. da Silva Filho, T. G. Bill, M. Malagoli, V. Coropceanu, A. Kahn, and J.-L. Brédas, "The vibrational reorganization energy in pentacene: Molecular influences on charge transport," *J. Am. Chem. Soc.*, vol. 124, no. 27, pp. 7918–7919, 2002.

[50] R. G. Kepler, "Charge carrier production and mobility in anthracene crystals," *Phys. Rev.*, vol. 119, no. 4, pp. 1226–1229, 1960.

[51] H. Klauk, M. Halik, U. Zschieschang, G. Schmid, W. Radlik, and W. Weber, "High-mobility polymer gate dielectric pentacene thin film transistors," *J. Appl. Phys.*, vol. 92, no. 9, pp. 5259–5263, 2002.

[52] V. Podzorov, S. E. Sysoev, E. Loginova, V. M. Pudalov, and M. E. Gershenson, "Single-crystal organic field effect transistors with the hole mobility ~8 cm^2/V s," *Appl. Phys. Let.*, vol. 83, no. 17, pp. 3504–3506, 2003.

[53] E. V. Tsiper and Z. G. Soos, "Electronic polarization in pentacene crystals and thin films," *Phys. Rev. B*, vol. 68, p. 085301, 2003.

[54] M. L. Tiago, J. E. Northrup, and S. G. Louie, "*Ab initio* calculation of the electronic and optical properties of solid pentacene," *Phys. Rev. B*, vol. 67, p. 115212, 2003.

[55] V. Lemaur, M. Steel, D. Beljonne, J.-L. Brédas, and J. Cornil, "Photoinduced charge generation and recombination dynamics in model donor/acceptor pairs for organic solar cell applications: A full quantum-chemical treatment," *J. Am. Chem. Soc.*, vol. 127, no. 16, pp. 6077–6085, 2005.

[56] A. Troisi, G. Orlandi, and J. E. Anthony, "Electronic interactions and thermal disorder in molecular crystals containing cofacial pentacene units," *Chem. Mater.*, vol. 17, pp. 5024–5031, 2005.

[57] T. Minari, T. Nemoto, and S. Isoda, "Fabrication and characterization of single-grain organic field-effect transistor of pentacene," *J. Appl. Phys.*, vol. 96, no. 1, pp. 769–772, 2004.

[58] C. R. Newman, R. J. Chesterfield, M. J. Panzer, and C. D. Frisbie, "High mobility top-gated pentacene thin-film transistors," *J. Appl. Phys.*, vol. 98, p. 084506, 2005.

[59] T. Minari, T. Nemoto, and S. Isoda, "Temperature and electric-field dependence of the mobility of a single-grain pentacene field-effect transistor," *J. Appl. Phys.*, vol. 99, p. 034506, 2006.

[60] A. Troisi and G. Orlandi, "Dynamics of the intermolecular transfer integral in crystalline organic semiconductors," *J. Phys. Chem. A*, vol. 110, pp. 4065–4070, 2006.

[61] J. C. Sancho-Garcia, G. Horowitz, J.-L. Brédas, and J. Cornil, "Effect of an external electric field on the charge transport parameters in organic molecular semiconductors," *J. Chem. Phys.*, vol. 119, pp. 12563–12568, 2003.

[62] W. J. Kim, W. H. Koo, S. J. Jo, C. S. Kim, H. K. Baik, J. Lee, and S. Im, "Encapsulation of organic field-effect transistors with highly polarizable transparent amorphous oxide," *Jap. J. of Appl. Phys.*, vol. 44, no. 37, pp. L1174–L1177, 2005.

[63] J. H. Lee, G. H. Kim, S. H. Kim, S. C. Lim, Y. S. Yang, J. H. Youk, J. Jang,

and T. Zyung, "Longevity enhancement of organic thin-film transistors by using a facile laminating passivation method," *Synth. Met.*, vol. 143, pp. 21–23, 2004.

[64] T. Cahyadi, J. N. Tey, S. G. Mhaisalkar, F. Boey, V. R. Rao, R. Lal, Z. H. Huang, G. J. Qi, Z.-K. Chen, and C. M. Ng, "Investigations of enhanced device characteristics in pentacene-based field effect transistors with sol-gel interfactial layer," *Appl. Phys. Let.*, vol. 90, p. 122112, 2007.

[65] C. Goldmann, D. J. Gundlach, and B. Batlogg, "Evidence of water-related discrete trap state formation in pentacene single-crystal field-effect transistors," *Appl. Phys. Let.*, vol. 88, p. 063501, 2006.

[66] G. Gu and M. G. Kane, "Moisture induced electron traps and hysteresis in pentacene-based organic thin-film transistors," *Appl. Phys. Let.*, vol. 92, p. 053305, 2008.

[67] T. Jung, A. Dodabalapur, R. Wenz, and S. Mohapatra, "Moisture induced surface polarization in a poly(4-vinyl phenol) dielectric in an organic thin-film transistor," *Appl. Phys. Let.*, vol. 87, p. 182109, 2005.

[68] O. D. Jurchescu, J. Baas, and T. T. M. Palstra, "Electronic transport properties of pentacene single crystals upon exposure to air," *Appl. Phys. Let.*, vol. 87, p. 052102, 2005.

[69] L. Tsetseris and S. T. Pantelides, "Intercalation of oxygen and water molecules in pentacene crystals: First-principles calculations," *Phys. Rev. B*, vol. 75, p. 153202, 2007.

[70] J. E. Northrup and M. L. Chabinyc, "Gap states in organic semiconductors: Hydrogen- and oxygen-induced states in pentacene," *Phys. Rev. B*, vol. 68, p. 041202, 2003.

[71] M. Jaquith, E. M. Muller, and J. A. Marohn, "Time-resolved electric force microscopy of charge trapping in polycrystalline pentacene," *J. Phys. Chem. B*, vol. 111, pp. 7711–7714, 2007.

[72] A. C. Mayer, R. Ruiz, R. L. Headrick, A. Kazimirov, and G. G. Malliaras, "Early stages of pentacene film growth on silicon oxide," *Org. Elec.*, vol. 5, pp. 257–263, 2004.

[73] S. Seo, L. C. Grabow, M. Mavrikakis, R. J. Hamers, N. J. Thompson, and

P. G. Evans, "Molecular-scale structural distortion near vacancies in pentacene," *Appl. Phys. Let.*, vol. 92, p. 153313, 2008.

[74] L. F. Drummy, C. Kubel, and D. C. Martinyk, "Molecular vacancies in herringbone crystals," *Philos. Mag.*, vol. 84, pp. 1955–1968, 2004.

[75] S. Verlaak, S. Steudel, P. Heremans, D. Janssen, and M. S. Deleuze, "Nucleation of organic semiconductors on inert substrates," *Phys. Rev. B*, vol. 68, p. 195409, 2003.

[76] Z.-T. Zhu, J. T. Mason, R. Dieckmann, and G. G. Malliaras, "Humidity sensors based on pentacene thin-film transistors," *Appl. Phys. Let.*, vol. 81, no. 24, pp. 4643–4645, 2002.

[77] D. H. Dunlap, P. E. Parris, and V. M. Kenkre, "Charge-dipole model for the universal field dependence of mobilities in molecularly doped polymers," *Phys. Rev. Let.*, vol. 77, no. 3, pp. 542–545, 1996.

[78] S. V. Novikov, D. H. Dunlap, V. M. Kenkre, P. E. Parris, and A. V. Vannikov, "Essential role of correlations in governing charge transport in disordered organic materials," *Phys. Rev. Let.*, vol. 81, no. 20, pp. 4472–4475, 1998.

[79] M. Pope and C. E. Swenberg, *Electronic Processes in Organic Crystals and Polymers*. New York: Oxford University Press, 1999.